Supplemental Information for:

# Investigating the electrocatalytic reduction of 2,4,6-tri-nitro-toluene (TNT) using density functional theory methods

Andrew Jark-Wah Wong, Joshua L. Miller, Brandon Perdue, and Michael J. Janik

Department of Chemical Engineering, the Pennsylvania State University, University Park, PA, USA

**Section S1: Benchmarking solvation energies of ionic species**

**Table S1** compares solvation energies of $CO_2H^-$ and $NH_4^+$ obtained from experiment and from the computational approaches we utilized. We chose these ions because the pKa values of $NH_4^+$ and $CO_2H_2$ are well known.

| ΔG of solvation of charged species in bulk solution (eV) | | | | |
|---|---|---|---|---|
| **Species** | **Experimental[1]** | **VASP/PBE/VASPSol** | **G16/B3LYP/IEFPCM** | **G16/PBEPBE/IEFPCM** |
| **$CO_2H^-$** | -4.18 | -2.76 | -2.84 | -2.79 |
| **$NH_4^+$** | -3.03 | -3.94 | -3.14 | -3.14 |

**Table S1:** Solvation energies of $CO_2H^-$ and $NH_4^+$ in bulk solution. Experimental solvation energies of ions are obtained from Marcus et al.[1] Solvation energies from DFT are obtained by taking the free energy difference of the system with solvation and the gas-phase system. Dielectric constant of bulk water and default implicit solvation parameters were used to model solvation in DFT. The 6-311G++g (d, p) basis set was used for all G16 calculations.

Both VASP/PBE/VASPSol and G16/IEFPCM/B3LYP under solvate anionic species by 1.42 and 1.34 eV, respectively. We ruled out functional differences as being negligible since difference in solvation energies between G16/B3LYP and G16/PBEPBE are small (0.05 eV). VASPSol over solvates the cationic species in bulk solution significantly by -0.9 eV while G16/IEFPCM approach under solvates slightly by 0.11 eV. Functional differences are negligible for cation species since energy differences between G16/B3LYP and G16/PBEPBE are identical. As a result, all outer-sphere energetics in the main text are reported using G16/B3LYP/IEFPCM due to higher accuracy achieved based on benchmarking with experimentally measured solvation energies. Solvation energies for coupled proton electron transferred species are nearly identical in VASPSol and IEFPCM, validating the use of VASPSol for inner-sphere solution phase species where all proton and electron transfers are coupled.

**Section S2:** Outer-sphere electrochemical reduction of TNT

**Figure S1:** VASP optimized geometries for reduced intermediates of TNT to O-$NH_2$-DNT outer-sphere electrochemical reduction. Atoms are presented as grey: C, white: H, blue: N, and red: O.

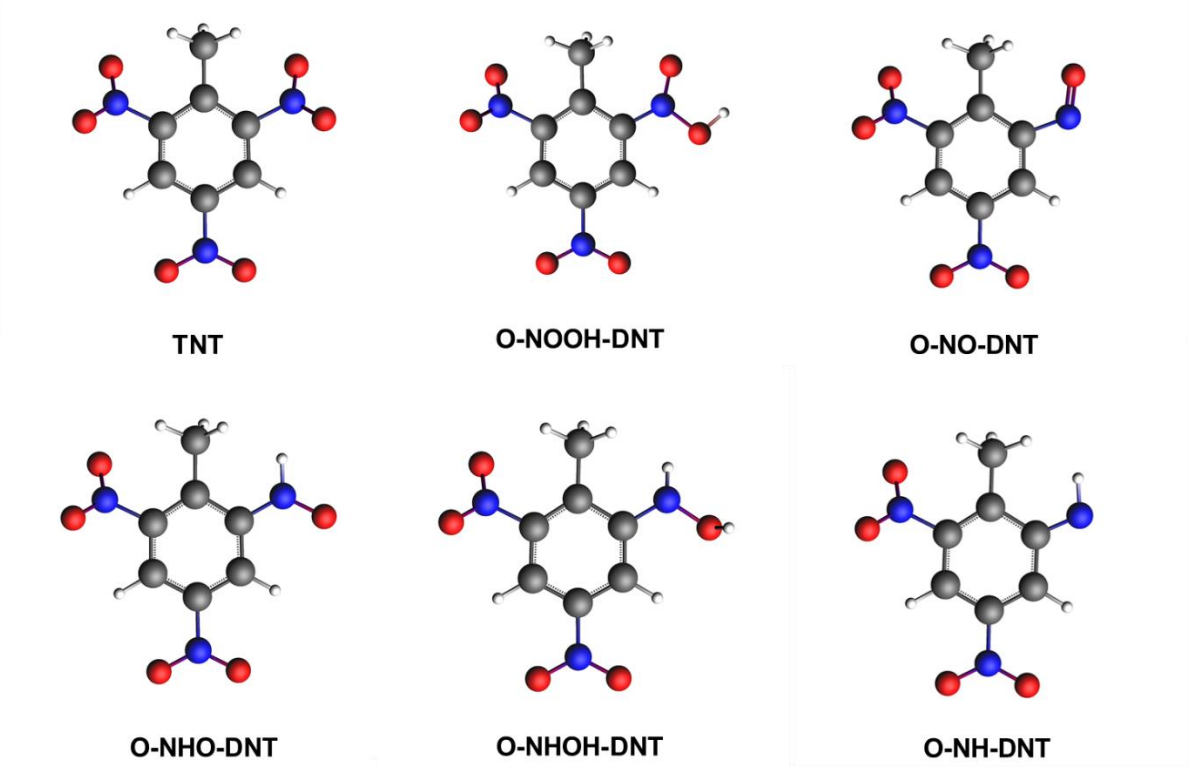

**Table S2:** Free energy change of reduction for the outer-sphere reduction of TNT to O-$NH_2$-DNT. Reaction energetics calculated in VASP utilized the PBE exchange-correlation functional and the VASPSol implicit solvation model. Reaction energetics calculated in Gaussian utilized the B3LYP exchange correlation functional, 6-311G++g(d,p) basis set, and the IEFPCM solvation model. All reaction energetics are referenced to TNT in the solution phase at 0 V-NHE and pH = 0.

| | **ΔG of reduction at 0 V-NHE and pH = 0 (eV)** | | | |
|---|---|---|---|---|
| **Species** | **VASP/PBE** | **G09/B3LYP** | **VASP/PBE/VASPSol** | **G09/B3LYP/IEFPCM** |
| **TNT-** | 1.64 | 1.74 | 0.62 | 0.24 |
| **O-NOOH-DNT+** | 3.42 | 4.11 | 0.66 | 1.85 |
| **O-NOOH-DNT** | 0.28 | 0.23 | 0.23 | 0.23 |
| **O-NOOH-DNT-** | 2.15 | 2.19 | 1.06 | 0.61 |
| **O-NO-DNT+** | 3.19 | 3.49 | 0.34 | 1.27 |
| **O-NO-DNT** | -0.94 | -1.06 | -0.88 | -1.02 |
| **O-NO-DNT-** | 0.54 | 0.55 | -0.52 | -0.94 |
| **O-NHO-DNT+** | 2.27 | 2.67 | -0.89 | 0.30 |
| **O-NHO-DNT** | -1.65 | -1.63 | -1.77 | -1.69 |
| **O-NHO-DNT-** | 0.11 | 0.39 | -1.61 | -1.32 |
| **O-NHOH-DNT+** | 1.88 | 2.09 | -1.58 | -0.35 |
| **O-NHOH-DNT** | -2.08 | -2.18 | -2.22 | -2.22 |
| **O-NHOH-DNT-** | 0.17 | 0.15 | -1.33 | -1.68 |
| **O-NH-DNT+** | 1.44 | 1.69 | -1.51 | -0.58 |
| **O-NH-DNT** | -2.97 | -2.95 | -2.95 | -2.94 |
| **O-NH-DNT-** | -1.67 | -1.60 | -2.82 | -3.16 |
| **O-$NH_2$-DNT+** | -0.51 | -0.19 | -3.64 | -2.55 |
| **O-$NH_2$-DNT** | -4.63 | -4.48 | -4.70 | -4.51 |

**Figure S2:** VASP optimized geometries for reduced intermediates of TNT to P-$NH_2$-DNT. Atoms are presented as grey: C, white: H, blue: N, and red: O.

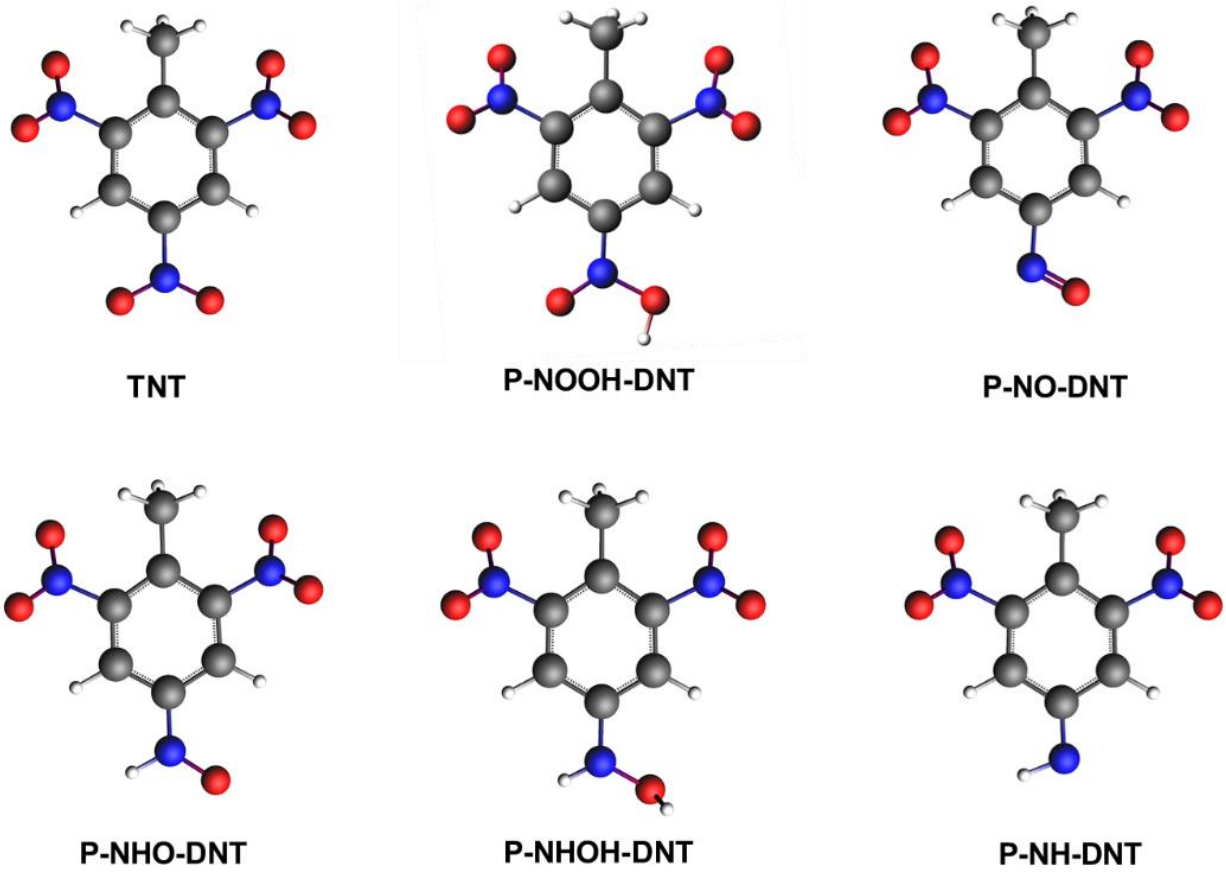

**Table S3:** Free energy change of reduction for the outer-sphere reduction of TNT to P-$NH_2$-DNT. Reaction energetics calculated in VASP utilized the PBE exchange-correlation functional and the VASPSol implicit solvation model. Reaction energetics calculated in Gaussian utilized the B3LYP exchange correlation functional, 6-311G++g (d, p) basis set, and the IEFPCM solvation model. All reaction energetics are referenced to TNT in the solution phase at 0 V-NHE and pH = 0.

| | **ΔG of reduction at 0 V-NHE and pH = 0 (eV)** | | | |
|---|---|---|---|---|
| **Species** | **VASP/PBE** | **G09/B3LYP** | **VASP/PBE/VASPSol** | **G09/B3LYP/IEFPCM** |
| **TNT-** | 1.64 | 1.74 | 0.62 | 0.24 |
| **P-NOOH.DNT+** | 3.42 | 4.07 | 0.61 | 1.84 |
| **P-NOOH-DNT** | 0.28 | 0.22 | 0.20 | 0.25 |
| **P-NOOH-DNT-** | 2.15 | 2.21 | 1.02 | 0.58 |
| **P-NO-DNT+** | 3.19 | 3.58 | 0.47 | 1.39 |
| **P-NO-DNT** | -0.94 | -1.42 | -0.88 | -0.99 |
| **P-NO-DNT-** | 0.54 | 0.59 | -0.56 | -0.97 |
| **P-NHO-DNT+** | 2.27 | 2.68 | -0.94 | 0.33 |
| **P-NHO-DNT** | -1.65 | -1.52 | -1.68 | -1.58 |
| **P-NHO-DNT-** | 0.27 | 0.77 | -1.47 | -1.12 |
| **P-NHOH-DNT+** | 1.88 | 2.12 | -1.53 | -0.27 |
| **P-NHOH-DNT** | -2.08 | -2.03 | -2.07 | -2.07 |
| **P-NHOH-DNT-** | 0.17 | 0.31 | -1.16 | -1.48 |
| **P-NH-DNT+** | 1.44 | 1.74 | -1.45 | -0.47 |
| **P-NH-DNT** | -2.97 | -2.81 | -2.83 | -2.79 |
| **P-NH-DNT-** | -1.67 | -1.37 | -2.60 | -0.95 |
| **P-$NH_2$-DNT+** | -0.51 | -0.16 | -3.59 | -2.17 |
| **P-$NH_2$-DNT** | **-4.63** | **-4.20** | **-4.53** | **-4.35** |

**Figure S3:** VASP optimized geometries for reduced intermediates of O-$NH_2$-DNT to P-$NO_2$-DAT. Reduction is initiated by reducing the ortho $NO_2$ group. Atoms are presented as grey: C, white: H, blue: N, and red: O.

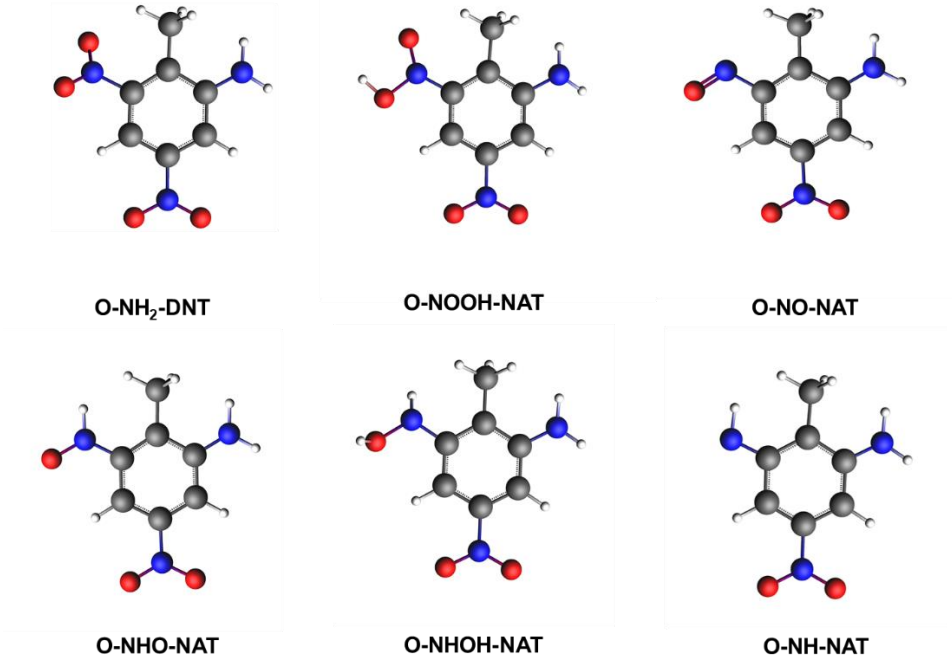

**Table S4:** Free energy change of reduction for the outer-sphere reduction of O-$NH_2$-DNT to P-$NO_2$-DAT. Reaction energetics calculated in VASP utilized the PBE exchange-correlation functional and the VASPSol implicit solvation model. Reaction energetics calculated in Gaussian utilized the B3LYP exchange correlation functional, 6-311G++g (d, p) basis set, and the IEFPCM solvation model. All reaction energetics are referenced to O-$NH_2$-DNT in the solution phase at 0 V-NHE and pH = 0.

| | **ΔG of reduction at 0 V-NHE and pH = 0 (eV)** | | | |
|---|---|---|---|---|
| **Species** | **VASP/PBE** | **G09/B3LYP** | **VASP/PBE/VASPSol** | **G09/B3LYP/IEFPCM** |
| **O-$NH_2$-DNT-** | 2.36 | 2.40 | 0.95 | 0.59 |
| **O-NOOH-NAT+** | 2.89 | 3.55 | 0.15 | 1.63 |
| **O-NOOH-NAT** | 0.45 | 0.32 | 0.51 | 0.35 |
| **O-NOOH-NAT-** | 2.92 | 2.89 | 1.49 | 0.93 |
| **O-NO-NAT+** | 2.58 | 3.09 | 0.04 | 0.94 |
| **O-NO-NAT** | -1.07 | -0.99 | -1.00 | -0.89 |
| **O-NO-NAT-1e** | 1.33 | 1.26 | -0.15 | -0.53 |
| **O-NHO-NAT+** | 1.76 | 2.03 | -1.00 | 0.02 |
| **O-NHO-NAT** | -1.37 | -1.36 | -1.50 | -1.55 |
| **O-NHO-NAT-** | 1.05 | 1.23 | -0.53 | -0.58 |
| **O-NHOH-NAT+** | **0.80** | 1.42 | -2.08 | -0.55 |
| **O-NHOH-NAT** | -1.98 | -1.96 | -2.08 | -1.99 |
| **O-NHOH-NAT-** | 1.49 | 1.19 | -0.52 | -1.14 |
| **O-NH-NAT+** | 0.76 | 0.98 | -1.92 | -0.98 |
| **O-NH-NAT** | -2.79 | -2.81 | -2.77 | -2.79 |
| **O-NH-NAT-** | -0.71 | -0.72 | -2.21 | -2.57 |
| **P-$NO_2$-DAT+** | -1.33 | -1.01 | -3.98 | -2.91 |
| **P-$NO_2$-DAT** | -4.39 | -4.25 | -4.41 | -4.24 |

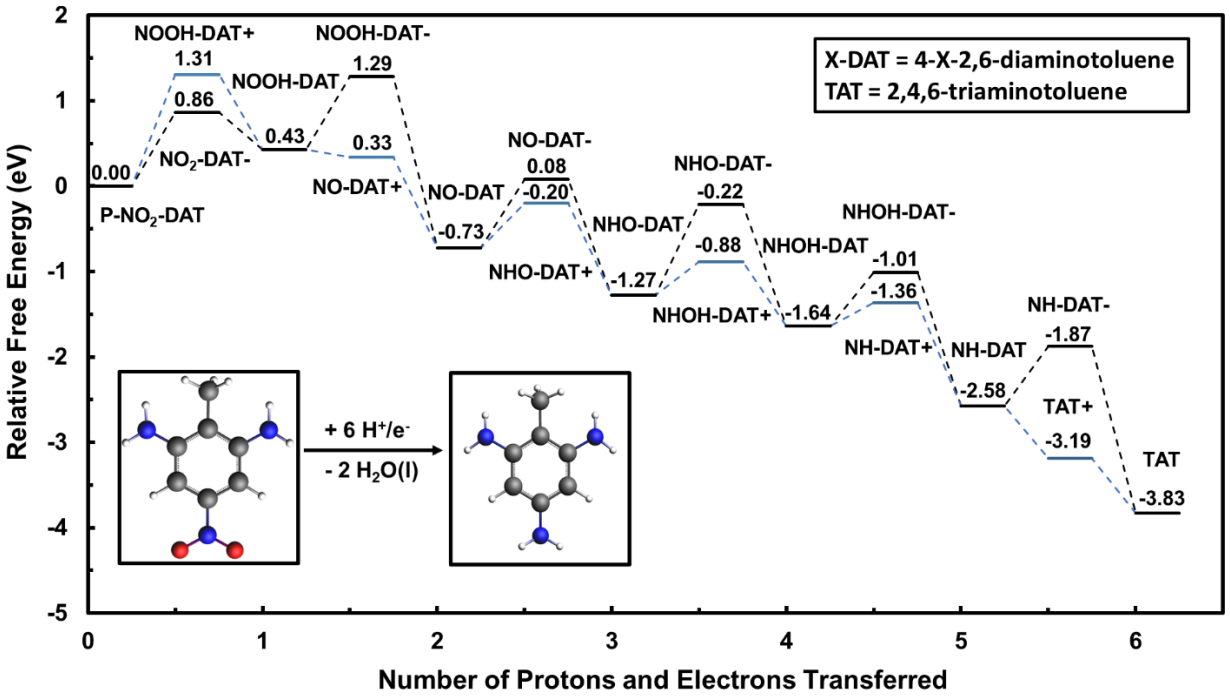


**Figure S4.** Reaction energy diagram for outer-sphere electrochemical reduction of P-$NO_2$-DAT to TAT in the solution phase, calculated using the G16 code with the IEFPCM continuum solvation model. The reduction initially proceeds by reducing the para $NO_2$ group of P-$NO_2$-DAT. Energies are relative to P-$NH_2$-DNT in the solution phase at 0 V-NHE and pH = 0. Water molecules formed during the reduction process are not listed on the diagram for clarity. Most stable configuration of each reduced intermediate is used. Black lines represent initial uncoupled electron transfer steps followed by proton transfer. Blue lines represent initial uncoupled proton transfer followed by electron transfer. Atom colors are presented as grey: C, white: H, blue: N, and red: O.

**Figure S5:** VASP optimized geometries for reduced intermediates of O-$NH_2$-DNT to O-$NO_2$-DAT. Reduction is initiated by reducing the para $NO_2$ group. Atoms are presented as grey: C, white: H, blue: N, and red: O.

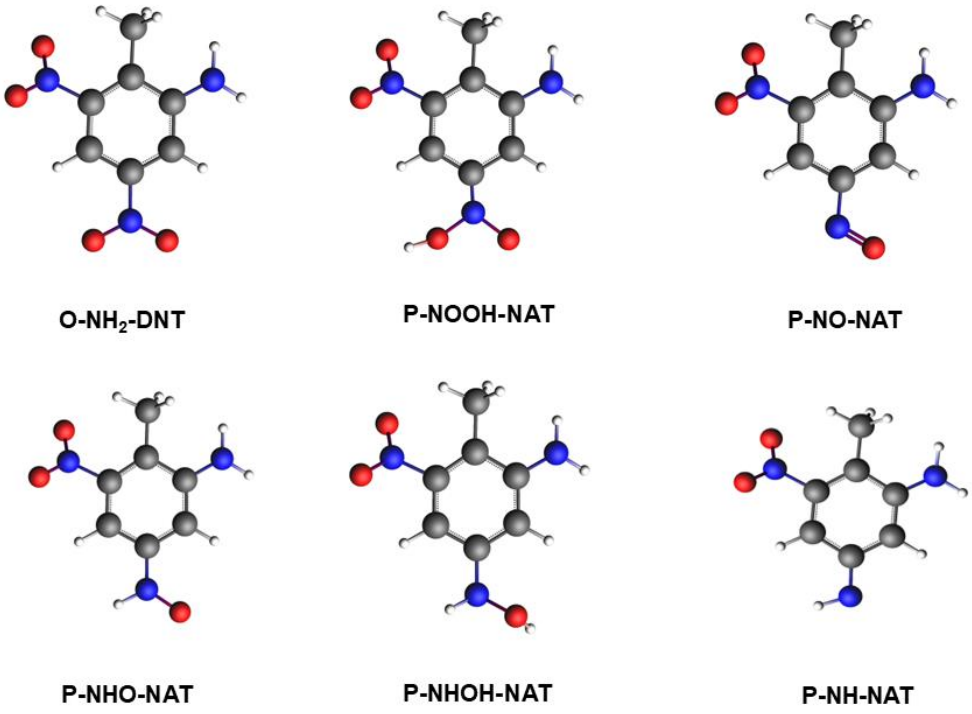

**Table S5:** Free energy change of reduction for outer-sphere reduction of O-$NH_2$-DNT to P-$NO_2$-DAT. Reaction energetics calculated in VASP utilized the PBE exchange-correlation functional and the VASPSol implicit solvation model. Reaction energetics calculated in Gaussian utilized the B3LYP exchange correlation functional, 6-311G++g (d, p) basis set, and the IEFPCM solvation model. All reaction energetics are referenced to O-$NH_2$-DNT in the solution phase at 0 V-NHE and pH = 0.

| | **ΔG of reduction at 0 V-NHE and pH = 0 (eV)** | | | |
|---|---|---|---|---|
| **Species** | **VASP/PBE** | **G09/B3LYP** | **VASP/PBE/VASPSol** | **G09/B3LYP/IEFPCM** |
| **O-$NH_2$-DNT-** | 2.57 | 2.40 | 0.95 | 0.13 |
| **P-NOOH-NAT+** | 2.78 | 3.80 | 0.09 | 1.37 |
| **P-NOOH-NAT** | 0.42 | 0.30 | 0.37 | -0.15 |
| **P-NOOH-NAT-** | 2.89 | 2.92 | 1.36 | 0.46 |
| **P-NO-NAT+** | 2.60 | 2.86 | 0.12 | 0.50 |
| **P-NO-NAT** | -0.95 | -0.99 | -0.93 | -1.40 |
| **P-NO-NAT-1e** | 1.36 | 1.30 | -0.09 | -1.01 |
| **P-NHO-NAT+** | 1.61 | 1.98 | -1.09 | -0.48 |
| **P-NHO-NAT** | -1.38 | -1.44 | -1.45 | -1.91 |
| **P-NHO-NAT-** | 1.08 | 1.30 | -0.44 | -1.10 |
| **P-NHOH-NAT+** | 0.70 | 1.35 | -2.13 | -1.05 |
| **P-NHOH-NAT** | -1.86 | -1.85 | -1.95 | -2.30 |
| **P-NHOH-NAT-** | 1.52 | 1.25 | -0.33 | -1.41 |
| **P-NH-NAT+** | 0.78 | 1.04 | -1.80 | -1.36 |
| **P-NH-NAT** | -2.70 | -2.70 | -2.67 | -3.11 |
| **P-NH-NAT-** | -0.56 | -0.53 | -2.04 | -2.85 |
| **O-$NO_2$-DAT+** | -1.35 | -0.99 | -3.95 | -3.37 |
| **O-$NO_2$-DAT** | -4.27 | -4.09 | -4.27 | -4.53 |

**Figure S6:** VASP optimized geometries for reduced intermediates of P-$NH_2$-DNT to O-$NO_2$-DAT. Reduction is initiated by reducing the ortho $NO_2$ group. Atoms are presented as grey: C, white: H, blue: N, and red: O.

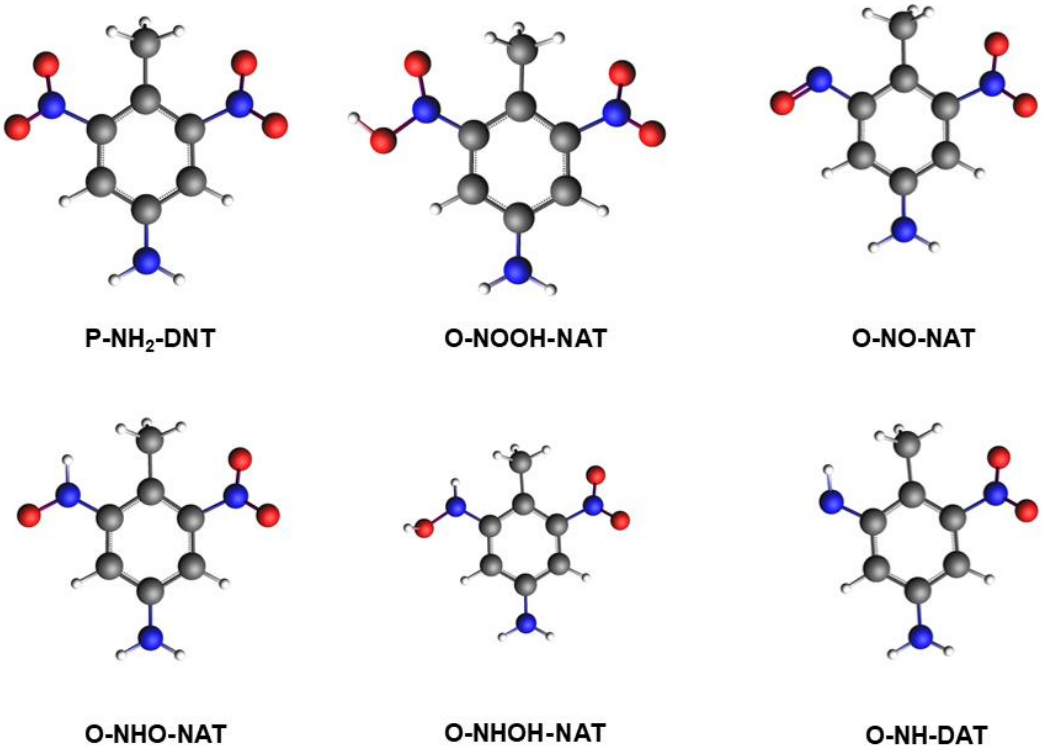

**Table S6:** Free energy change of reduction for outer-sphere reduction of P-$NH_2$-DNT to O-$NO_2$-DAT. Reaction energetics calculated in VASP utilized the PBE exchange-correlation functional and the VASPSol implicit solvation model. Reaction energetics calculated in Gaussian utilized the B3LYP exchange correlation functional, 6-311G++g(d, p) basis set, and the IEFPCM solvation model. All reaction energetics are referenced to P-$NH_2$-DNT in the solution phase at 0 V-NHE and pH = 0.

| | **ΔG of reduction at 0 V-NHE and pH = 0 (eV)** | | | |
|---|---|---|---|---|
| **Species** | **VASP/PBE** | **G09/B3LYP** | **VASP/PBE/VASPSol** | **G09/B3LYP/IEFPCM** |
| **P-$NH_2$-DNT-** | 2.39 | 2.59 | 0.99 | 0.85 |
| **O-NOOH-NAT+** | 2.77 | 3.35 | 0.09 | 1.60 |
| **O-NOOH-NAT** | 0.44 | 0.22 | 0.40 | 0.36 |
| **O-NOOH-NAT-** | 2.91 | 2.81 | 1.47 | 0.97 |
| **O-NO-NAT+** | 2.43 | 2.58 | -0.07 | -5.24 |
| **O-NO-NAT** | -1.08 | -1.24 | -1.02 | -1.05 |
| **O-NO-NAT-1e** | 1.19 | 0.98 | -0.23 | -0.69 |
| **O-NHO-NAT+** | 1.56 | 1.80 | -1.11 | -0.09 |
| **O-NHO-NAT** | -1.49 | -1.67 | -1.54 | -1.55 |
| **O-NHO-NAT-** | 0.92 | 1.01 | -0.61 | -0.82 |
| **O-NHOH-NAT+** | 0.53 | 1.01 | -2.23 | -0.70 |
| **O-NHOH-NAT** | -2.04 | -2.11 | -2.10 | -1.98 |
| **O-NHOH-NAT-** | 1.40 | 1.03 | -0.47 | -1.09 |
| **O-NH-NAT+** | 0.61 | 0.68 | -1.96 | -1.12 |
| **O-NH-NAT** | -2.86 | -3.01 | -2.82 | -2.84 |
| **O-NH-NAT-** | -0.72 | -0.89 | -2.19 | -2.59 |
| **O-$NO_2$-DAT+** | -1.52 | -1.27 | -4.12 | -3.07 |
| **O-$NO_2$-DAT** | -4.44 | -4.37 | -4.43 | -4.23 |

**Figure S7:** VASP optimized geometries for reduced intermediates of P-$NO_2$-DAT to TAT. Reduction is initiated by reducing the ortho $NO_2$ group. Atoms are presented as grey: C, white: H, blue: N, and red: O.

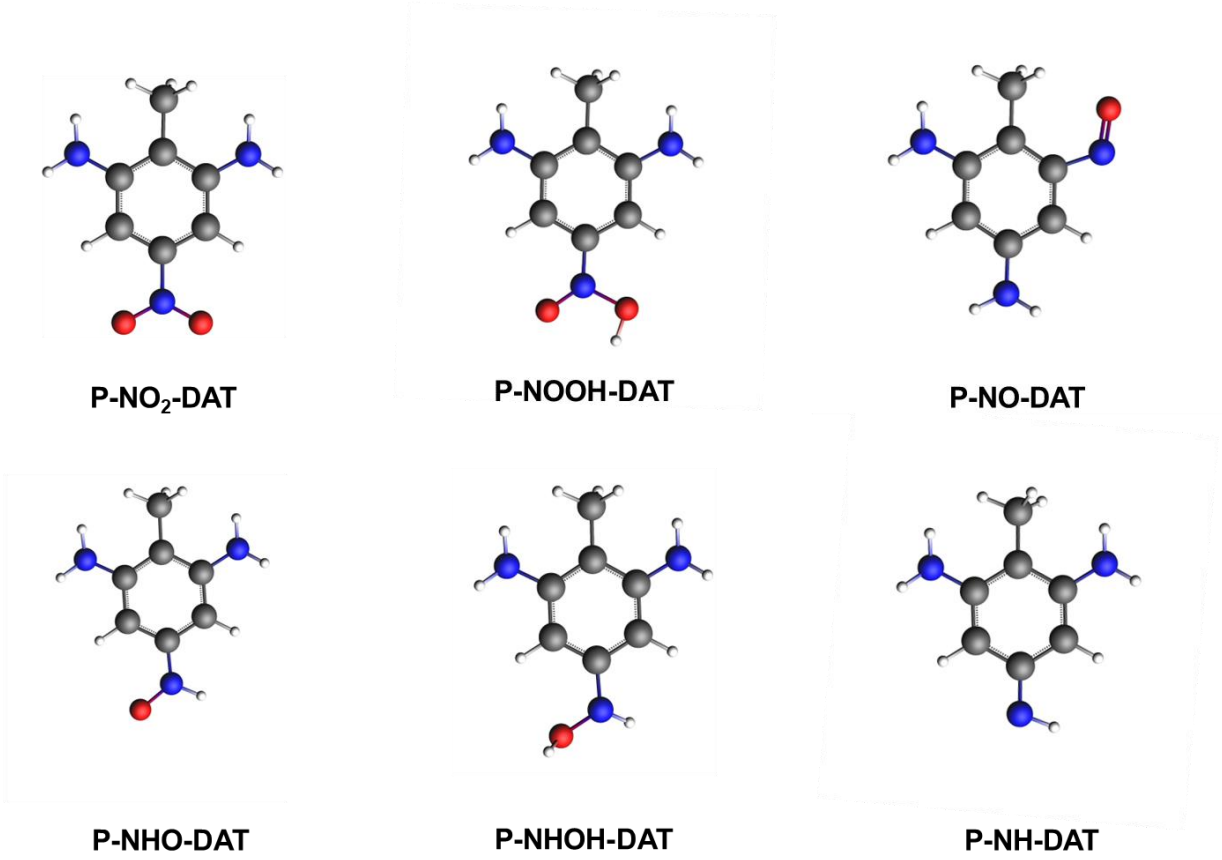

**Table S7:** Free energy change of reduction for outer-sphere reduction of P-$NO_2$-DAT to TAT. Reaction energetics calculated in VASP utilized the PBE exchange-correlation functional and the VASPSol implicit solvation model. Reaction energetics calculated in Gaussian utilized the B3LYP exchange correlation functional, 6-311G++g (d, p) basis set, and the IEFPCM solvation model. All reaction energetics are referenced to P-$NO_2$-DAT in the solution phase at 0 V-NHE and pH = 0.

| | **ΔG of reduction at 0 V-NHE and pH = 0 (eV)** | | | |
|---|---|---|---|---|
| **Species** | **VASP/PBE** | **G09/B3LYP** | **VASP/PBE/VASPSol** | **G09/B3LYP/IEFPCM** |
| **P-$NO_2$-DAT-** | 3.42 | 3.22 | 1.47 | 0.86 |
| **P-NOOH-$DAT_+$** | 2.17 | 2.87 | -0.10 | 1.31 |
| **P-NOOH-DAT** | 0.67 | 0.39 | 0.60 | 0.43 |
| **P-NOOH-DAT-** | 3.74 | 3.61 | 1.71 | 1.29 |
| **P-NO-DAT+** | 1.92 | 2.29 | -0.38 | 0.34 |
| **P-NO-DAT** | -0.73 | -0.94 | -0.73 | -0.73 |
| **P-NO-DAT-** | 2.34 | 2.15 | 0.37 | 0.08 |
| **P-NHO-DAT+** | 1.03 | 1.37 | -1.30 | -0.20 |
| **P-NHO-DAT** | -1.14 | -1.32 | -1.22 | -1.27 |
| **P-NHO-DAT-** | 2.21 | 2.29 | 0.28 | -0.22 |
| **P-NHOH-DAT+** | 0.71 | 0.77 | -1.50 | -5.92 |
| **P-NHOH-DAT** | -1.43 | -1.67 | -1.48 | -1.64 |
| **P-NHOH-DAT-** | 2.40 | 2.94 | 1.79 | 1.39 |
| **P-NH-DAT+** | 0.12 | 0.32 | -2.32 | -1.36 |
| **P-NH-DAT** | -2.63 | -2.60 | -2.57 | -2.58 |
| **P-NH-DAT-** | 0.34 | 0.32 | -1.51 | -1.87 |
| **TAT+** | -1.75 | -1.62 | -3.70 | -3.19 |
| **TAT** | -3.90 | -3.90 | -3.85 | -3.83 |

**Figure S8:** VASP optimized geometries for reduced intermediates of O-$NO_2$-DAT to TAT. Reduction is initiated by reducing the ortho $NO_2$ group. Atoms are presented as grey: C, white: H, blue: N, and red: O.

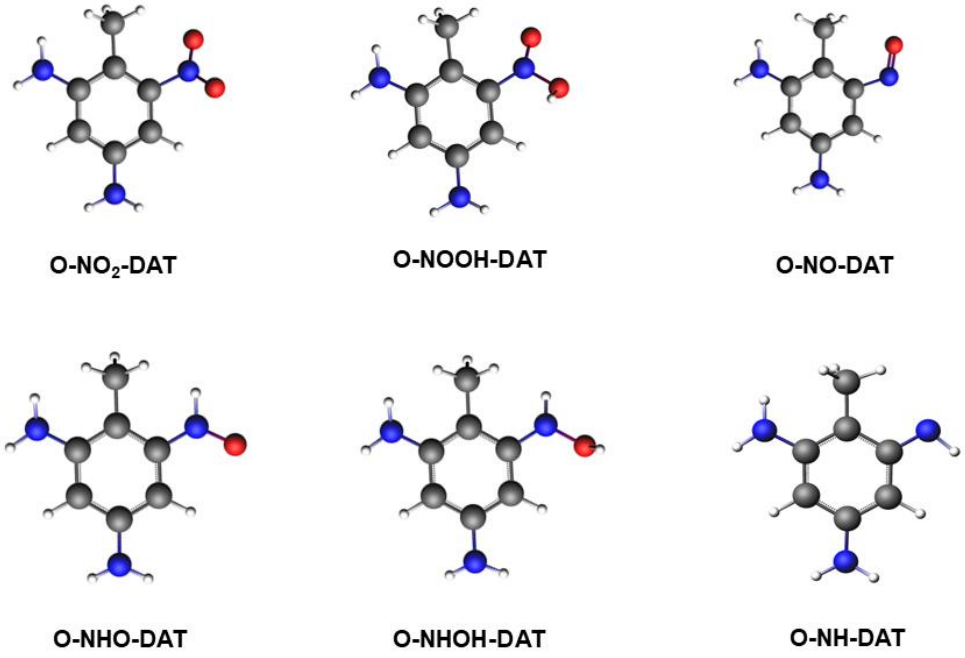

**Table S8:** Free energy change of reduction for outer-sphere reduction of O-$NO_2$-DAT to TAT. Reaction energetics calculated in VASP utilized the PBE exchange-correlation functional and the VASPSol implicit solvation model. Reaction energetics calculated in Gaussian utilized the B3LYP exchange correlation functional, 6-311G++g (d, p) basis set, and the IEFPCM solvation model. All reaction energetics are referenced to O-$NO_2$-DAT in the solution phase at 0 V-NHE and pH = 0.

| | **ΔG of reduction at 0 V-NHE and pH = 0 (eV)** | | | |
|---|---|---|---|---|
| **Species** | **VASP/PBE** | **G09/B3LYP** | **VASP/PBE/VASPSol** | **G09/B3LYP/IEFPCM** |
| **P-$NO_2$-DAT-** | 3.44 | 3.22 | 1.57 | 0.95 |
| **P-NOOH-$DAT_+$** | 2.42 | 3.14 | 0.07 | 1.46 |
| **P-NOOH-DAT** | 0.84 | 0.42 | 0.70 | 0.50 |
| **P-NOOH-DAT-** | 3.74 | 3.59 | 1.58 | 2.05 |
| **P-NO-DAT+** | 1.79 | 2.34 | -0.50 | 0.16 |
| **P-NO-DAT** | -0.72 | -0.96 | -0.70 | -0.90 |
| **P-NO-DAT-** | 2.34 | 2.13 | 0.44 | -0.10 |
| **P-NHO-DAT+** | 1.00 | 1.28 | -1.33 | -0.37 |
| **P-NHO-DAT** | -1.23 | -1.43 | -1.31 | -1.45 |
| **P-NHO-DAT-** | 2.02 | 1.94 | 0.09 | -0.39 |
| **P-NHOH-DAT+** | 0.55 | 0.57 | -1.75 | -1.06 |
| **P-NHOH-DAT** | -1.56 | -1.80 | -1.61 | -1.79 |
| **P-NHOH-DAT-** | 2.27 | 2.79 | 1.68 | -1.18 |
| **P-NH-DAT+** | 0.00 | 0.07 | -2.30 | -1.57 |
| **P-NH-DAT** | -2.76 | -2.81 | -2.71 | -2.75 |
| **P-NH-DAT-** | 0.20 | 0.04 | -1.78 | -2.07 |
| **TAT+** | -1.88 | -1.78 | -3.84 | -3.36 |
| **TAT** | -4.03 | -4.06 | -3.99 | -4.00 |

**Section S3: Electrocatalytic reduction of TNT on the Fe (110) surface**

**Figure S9:** Optimized geometries for intermediates from TNT to O-$NH_2$-DNT reduction on the Fe (110) surface. TNT is adsorbed and reduced through the ortho group. Atom colors are presented as brown: Fe, grey: C, blue: N, red: O, and white: H.

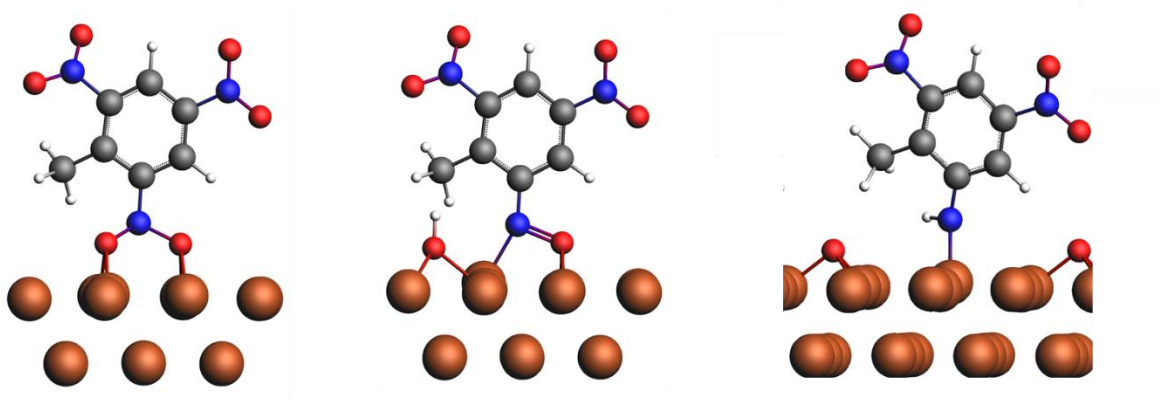


**Table S9:** Free energy change of reduction for the electrocatalytic reduction of TNT to O-$NH_2$-DNT on the Fe (110) surface. Reaction energetics were calculated in VASP using the VASPSol implicit solvation model. All reaction energetics are referenced to TNT and the Fe (110) surface in the solution phase at 0 V-RHE.

| Species | ΔG of reduction at 0 V-RHE (eV) |
|---|---|
| TNT* (O-Adsorbed) | -1.57 |
| O-NO-DNT* + OH* | -3.90 |
| O-NO-DNT | -3.15 |
| O-NH-DNT* + O* | -5.60 |
| O-$NH_2$-DNT(aq) + O* | -5.60 |
| O-$NH_2$-DNT(aq) + OH* | -5.44 |
| O-$NH_2$-DNT(aq) | -4.70 |

**Figure S10:** Reaction energy diagram for electrocatalytic reduction of TNT to O-$NH_2$-DNT on the Fe (110) surface at 0 V-RHE. Energies are relative to the bare solvated surface and TNT in the solution phase. TNT reduction is initiated through the flat adsorption configuration on the Fe (110) surface. Water molecules formed during the reduction process are not listed on the diagram for clarity. Most stable configuration of each reduced intermediate are used to construct the reaction energy diagram. Water molecules formed during the reduction of TNT are not depicted for clarity. Black lines represent free energies of stable TNT intermediates. Atom colors are presented as brown: Fe grey: C, white: H, blue: N, and red: O

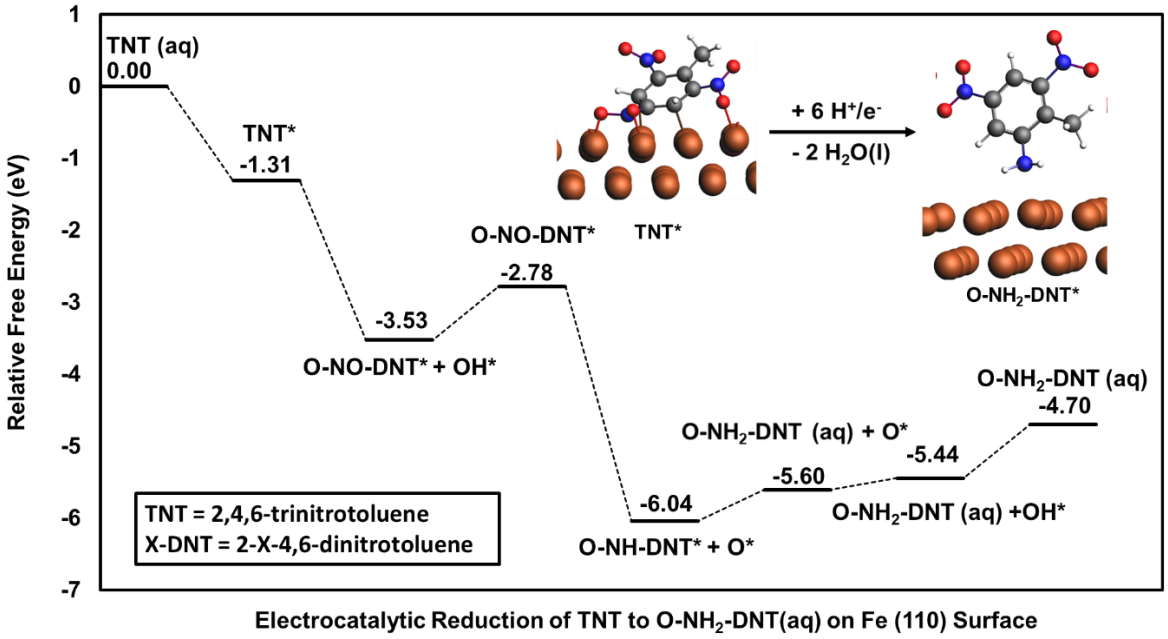


**Figure S11:** Optimized geometries for intermediates from TNT to O-$NH_2$-DNT reduction on the Fe (110) surface. TNT is adsorbed in the flat configuration and reduced through the ortho group. Atom colors are presented as brown: Fe, grey: C, blue: N, red: O, and white: H.

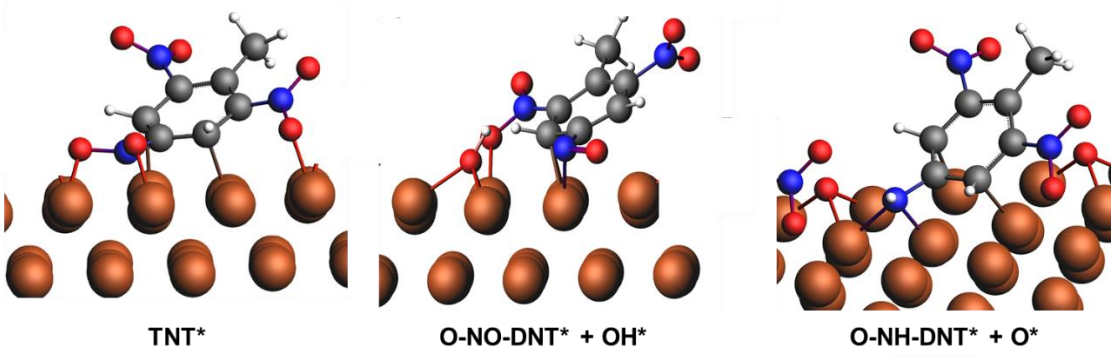

**Figure S12:** Optimized geometries for intermediates from TNT to P-$NH_2$-DNT reduction on the Fe (110) surface. TNT is adsorbed and reduced through the para group. Atoms are presented as brown: Fe, grey: C, white: H, blue: N, and red: O.

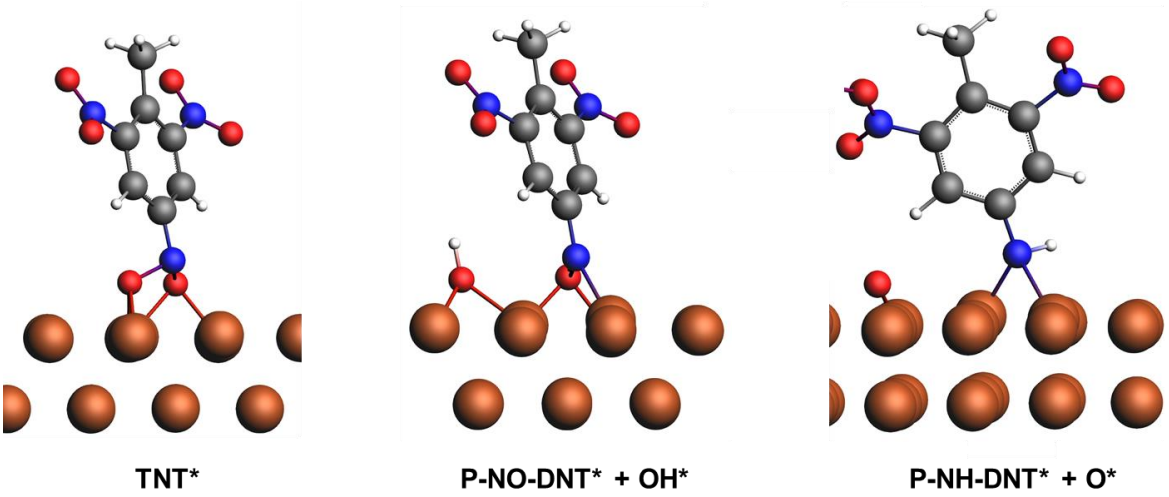


**Table S10:** Free energy change of reduction for the electrocatalytic reduction of TNT to P-$NH_2$-DNT on the Fe (110) surface. Reaction energetics were calculated in VASP using the VASPSol implicit solvation model. All reaction energetics are referenced to TNT and the Fe (110) surface in the solution phase at 0 V-RHE.

| Species | ΔG of reduction at 0 V-RHE (eV) |
|---|---|
| TNT* (P-Adsorbed) | -1.46 |
| P-NO-DNT* + OH* | -3.58 |
| P-NO-DNT | -2.83 |
| P-NH-DNT* + O* | -5.65 |
| P-$NH_2$-DNT (aq) + O* | -5.44 |
| P-$NH_2$-DNT (aq) + OH* | -5.28 |
| P-$NH_2$-DNT (aq) | -4.53 |

**Figure S13:** Optimized geometries for reduced intermediates of O-$NH_2$-DNT to P-$NO_2$-DAT on the Fe (110) surface. O-$NH_2$-DNT is adsorbed and reduced through the ortho group. Atoms are presented as brown: Fe, grey: C, white: H, blue: N, and red: O.

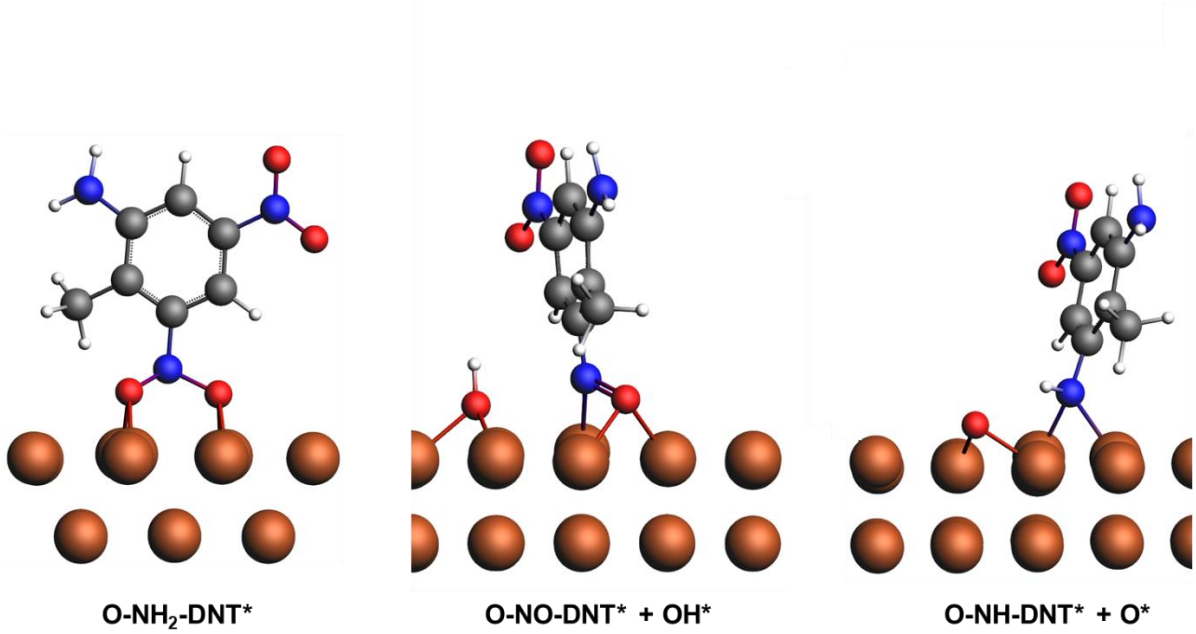


**Table S11:** Free energy change of reduction for the electrocatalytic reduction of O-$NH_2$-DNT to P-$NO_2$-DAT on the Fe (110) surface. Reaction energetics were calculated in VASP using the VASPSol implicit solvation model. All reaction energetics are referenced to O-$NH_2$-DNT and the Fe (110) surface in the solution phase at 0 V-RHE.

| Species | ΔG of reduction at 0 V-RHE (eV) |
|---|---|
| O-$NH_2$-DNT* (O Ads) | -1.33 |
| O-NO-NAT* + OH* | -3.24 |
| O-NO-NAT* | -2.49 |
| O-NH-NAT* + O* | -5.26 |
| P-$NO_2$-DAT (aq) + O* | -5.32 |
| P-$NO_2$-DAT (aq) + OH* | -5.15 |
| P-$NO_2$-DAT (aq) | -4.41 |

**Figure S14:** Optimized geometries for reduced intermediates of O-$NH_2$-DNT to O-$NO_2$-DAT on the Fe (110) surface. O-$NH_2$-DNT is adsorbed and reduced through the para group. Atoms are presented as brown: Fe, grey: C, white: H, blue: N, and red: O.

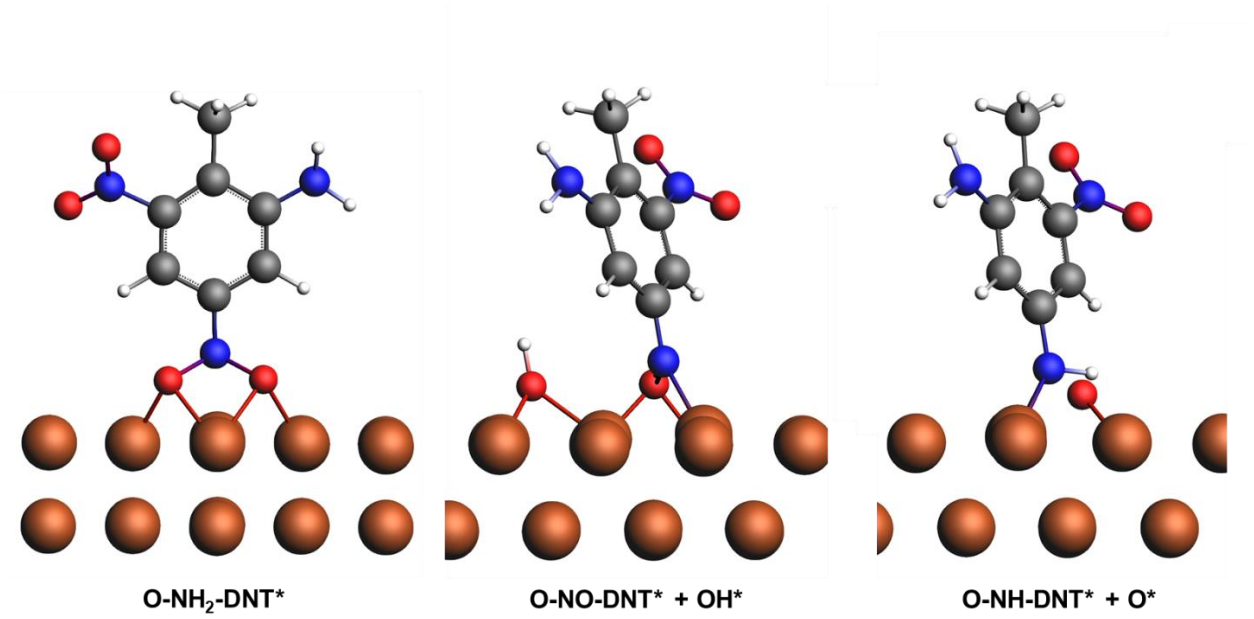


**Table S12:** Free energy change of reduction for the electrocatalytic reduction of O-$NH_2$-DNT to O-$NO_2$-DAT on the Fe (110) surface. Reaction energetics were calculated in VASP using the VASPSol implicit solvation model. All reaction energetics are referenced to O-$NH_2$-DNT and the Fe (110) surface in the solution phase at 0 V-RHE.

| Species | ΔG of reduction at 0 V-RHE (eV) |
|---|---|
| O-$NH_2$-DNT* (P Ads) | -1.33 |
| P-NO-NAT* + OH* | -3.24 |
| P-NO-NAT* | -2.49 |
| P-NH-NAT* + O* | -5.47 |
| O-$NO_2$-DAT (aq) + O* | -5.18 |
| O-$NO_2$-DAT (aq) + OH* | -5.02 |
| O-$NO_2$-DAT (aq) | -4.27 |

**Figure S15:** Optimized geometries for reduced intermediates of P-$NH_2$-DNT to O-$NO_2$-DAT on the Fe (110) surface. P-$NH_2$-DNT is adsorbed and reduced through the ortho group. Atoms are presented as brown: Fe, grey: C, white: H, blue: N, and red: O.

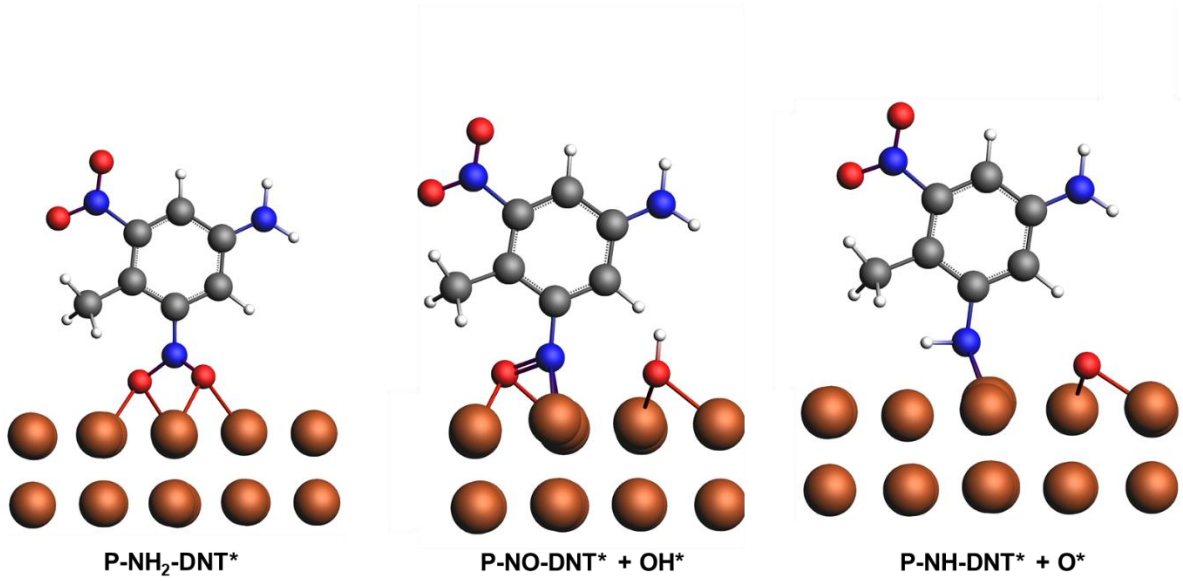


**Table S13:** Free energy change of reduction for the electrocatalytic reduction of P-$NH_2$-DNT to O-$NO_2$-DAT on the Fe (110) surface. Reaction energetics were calculated in VASP using the VASPSol implicit solvation model. All reaction energetics are referenced to P-$NH_2$-DNT and the Fe (110) surface in the solution phase at 0 V-RHE.

| Species | ΔG of reduction at 0 V-RHE (eV) |
|---|---|
| P-$NH_2$-DNT* (O ads) | -1.62 |
| O-NO-NAT* + OH* | -3.47 |
| O-NO-NAT* | -2.73 |
| O-NH-NAT* + O* | -5.41 |
| O-$NO_2$-DAT (aq) + O* | -5.34 |
| O-$NO_2$-DAT (aq) + OH* | -5.18 |
| O-$NO_2$-DAT (aq) | -4.43 |

**Figure S16:** Optimized geometries for reduced intermediates of P-$NO_2$-DAT to TAT on the Fe (110) surface. P-$NO_2$-DAT is adsorbed and reduced through the para group. Atoms are presented as grey: C, white: H, blue: N, and red: O.

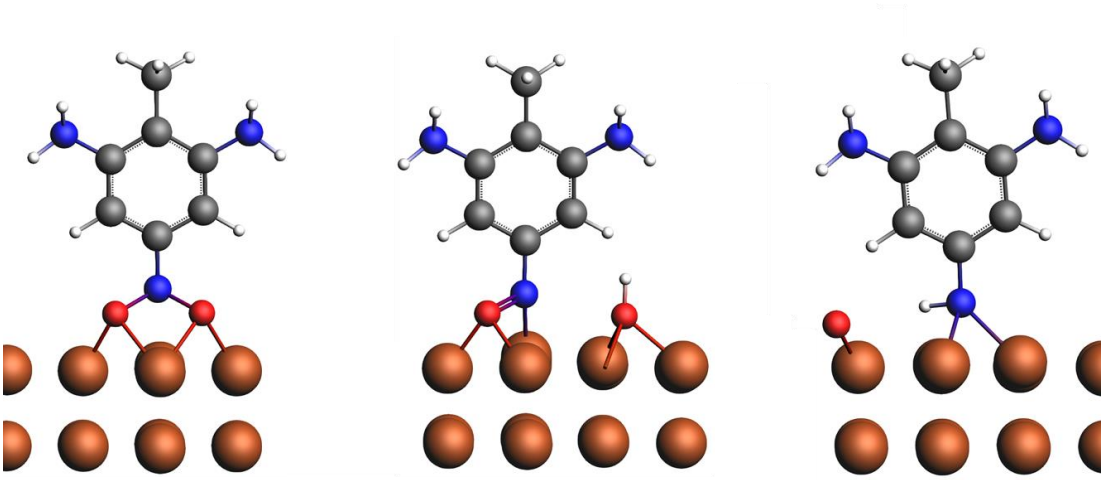


**Table S14:** Free energy change of reduction for the electrocatalytic reduction of P-$NO_2$-DAT to TAT on the Fe (110) surface. Reaction energetics were calculated in VASP using the VASPSol implicit solvation model. All reaction energetics are referenced to P-$NO_2$-DAT and the Fe (110) surface in the solution phase at 0 V-RHE.

| Species | ΔG of reduction at 0 V-RHE (eV) |
|---|---|
| P-$NO_2$-DAT* | -1.31 |
| P-NO-DAT* + OH* | -3.32 |
| P-NO-DAT* | -2.58 |
| P-NH-DAT* + O* | -5.10 |
| TAT (aq) + O* | -4.76 |
| TAT (aq) + OH* | -4.60 |
| TAT (aq) | -3.85 |

**Figure S17:** Optimized geometries for reduced intermediates of O-$NO_2$-DAT to TAT on the Fe (110) surface. O-$NO_2$-DAT is adsorbed and reduced through the ortho group. Atoms are presented as grey: C, white: H, blue: N, and red: O.

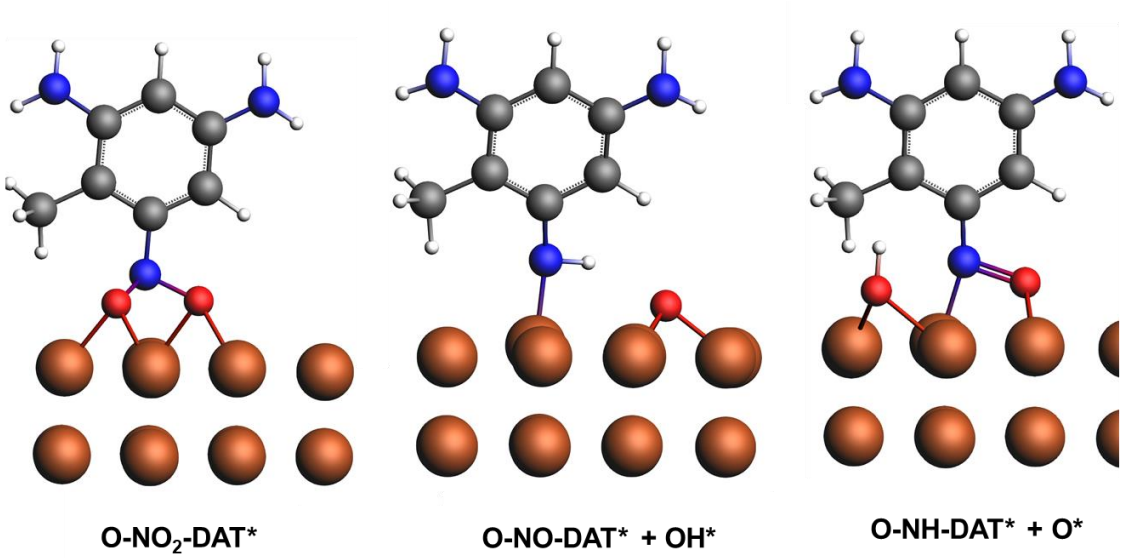


**Table S15:** Free energy change of reduction for the electrocatalytic reduction of O-$NO_2$-DAT to TAT on the Fe (110) surface. Reaction energetics were calculated in VASP using the VASPSol implicit solvation model. All reaction energetics are referenced to O-$NO_2$-DAT and the Fe (110) surface in the solution phase at 0 V-RHE.

| Species | ΔG of reduction at 0 V-RHE (eV) |
|---|---|
| O-$NO_2$-DAT* | -0.87 |
| O-NO-DAT* + OH* | -3.30 |
| O-NO-DAT* | -2.56 |
| O-NH-DAT* + O* | -5.08 |
| TAT (aq) + O* | -4.90 |
| TAT (aq) + OH* | -4.74 |
| TAT (aq) | -3.99 |

**Section S4: Electrocatalytic reduction of TNT on the Au (111) surface**

**Figure S18:** Optimized geometries for intermediates from TNT to O-$NH_2$-DNT reduction on the Au (111) surface. Atom colors are presented as yellow: Au, grey: C, blue: N, red: O, and white: H.

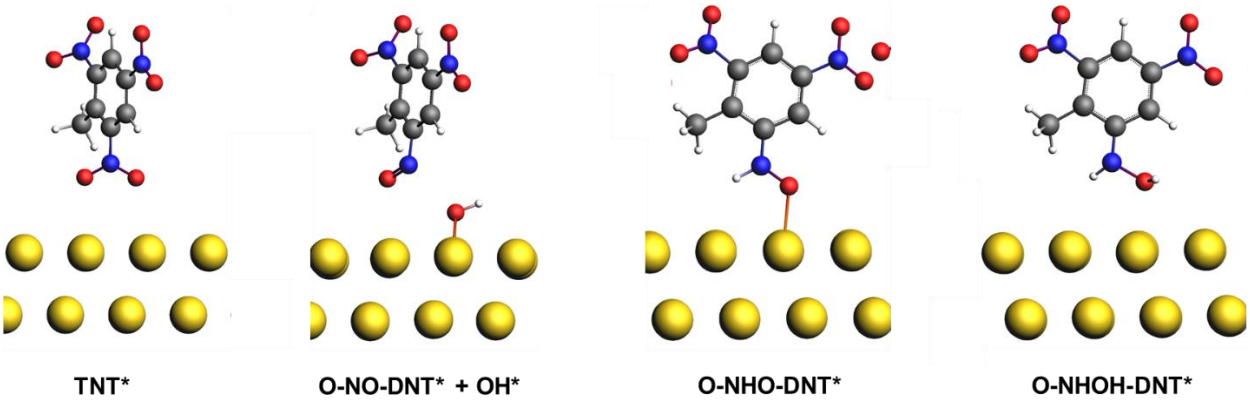


**Table S16:** Free energy change of reduction for the electrocatalytic reduction of TNT to O-$NH_2$-DNT on the Au (111) surface. Reaction energetics were calculated in VASP using the VASPSol implicit solvation model. All reaction energetics are referenced to TNT and the Au (111) surface in the solution phase at 0 V-RHE.

| Species | ΔG of reduction at 0 V-RHE (eV) |
|---|---|
| TNT* | -0.19 |
| O-NO-DNT* + OH* | 0.51 |
| O-NO-DNT* | -0.94 |
| O-NHO-DNT* | -1.53 |
| O-NHOH-DNT* | -2.31 |
| O-$NH_2$-DNT (aq) + OH* | -3.25 |
| O-$NH_2$-DNT (aq) | -4.70 |

**Figure S19:** Optimized geometries for intermediates from TNT to P-$NH_2$-DNT reduction on the Au (111) surface. TNT is adsorbed and reduced through the para group. Atom colors are presented as yellow: Au, grey: C, blue: N, red: O, and white: H.

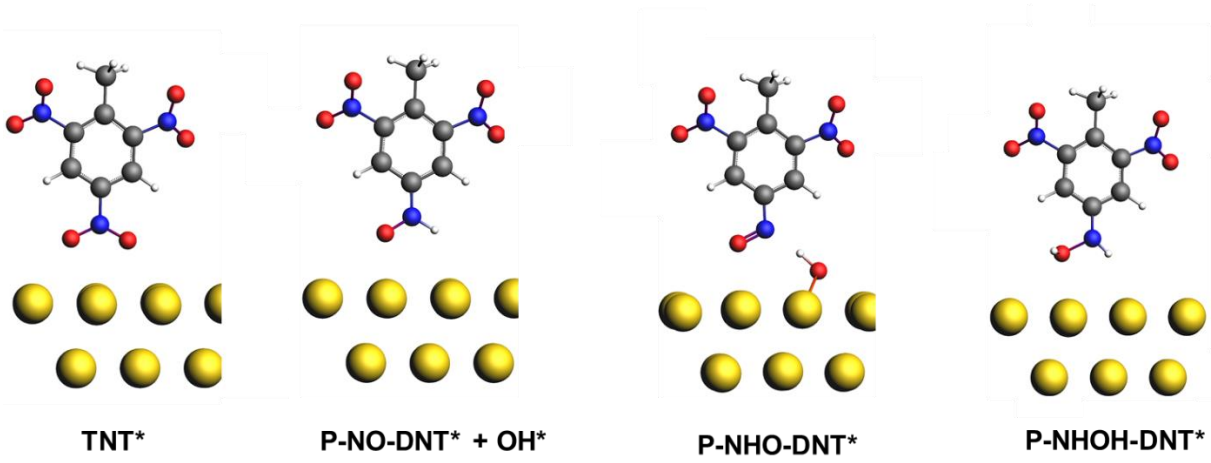


**Table S17:** Free energy change of reduction for the electrocatalytic reduction of TNT to P-$NH_2$-DNT on the Au (111) surface. Reaction energetics were calculated in VASP using the VASPSol implicit solvation model. All reaction energetics are referenced to TNT and the Au (111) surface in the solution phase at 0 V-RHE.

| Species | ΔG of reduction at 0 V-RHE (eV) |
|---|---|
| TNT* | -0.02 |
| P-NO-DNT* + OH* | 0.48 |
| P-NO-DNT* | -0.96 |
| P-NHO-DNT* | -1.50 |
| P-NHOH-DNT* | -1.95 |
| P-$NH_2$-DNT (aq) + OH* | -3.08 |
| P-$NH_2$-DNT (aq) | -4.53 |

**Figure S20:** Optimized geometries for reduced intermediates of O-$NH_2$-DNT to P-$NO_2$-DAT on the Au (111) surface. O-$NH_2$-DNT is adsorbed and reduced through the ortho group. Atom colors are presented as yellow: Au, grey: C, blue: N, red: O, and white: H.

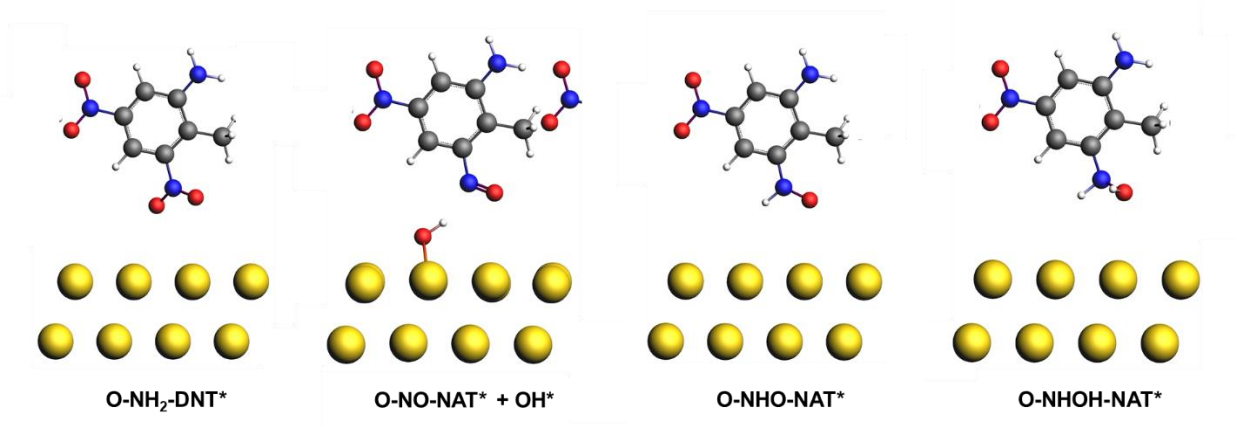


**Table S18:** Free energy change of reduction for the electrocatalytic reduction of O-$NH_2$-DNT to P-$NO_2$-DAT on the Au (111) surface. Reaction energetics were calculated in VASP using the VASPSol implicit solvation model. All reaction energetics are referenced to O-$NH_2$-DNT and the Au (111) surface in the solution phase at 0 V-RHE.

| Species | ΔG of reduction at 0 V-RHE (eV) |
|---|---|
| O-$NH_2$-DNT* | -0.02 |
| O-NO-NAT* + OH* | 0.56 |
| O-NO-NAT* | -0.89 |
| O-NHO-NAT* | -1.33 |
| O-NHOH-NAT* | -1.94 |
| P-$NO_2$-DAT (aq) + OH* | -2.82 |
| P-$NO_2$-DAT (aq) | -4.27 |

**Figure S21:** Optimized geometries for reduced intermediates of O-$NH_2$-DNT to O-$NO_2$-DAT on the Au (111) surface. O-$NH_2$-DNT is adsorbed and reduced through the para group. Atom colors are presented as yellow: Au, grey: C, blue: N, red: O, and white: H.

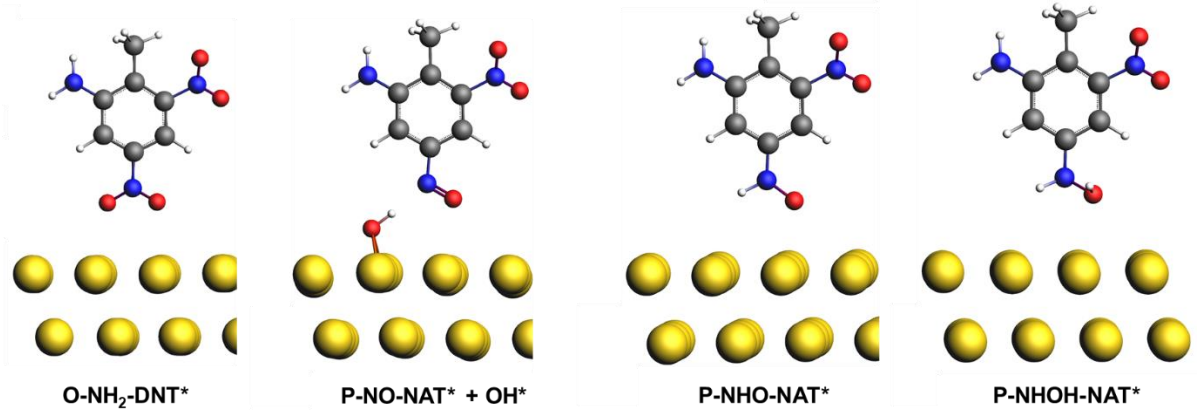


**Table S19:** Free energy change of reduction for the electrocatalytic reduction of O-$NH_2$-DNT to O-$NO_2$-DAT on the Au (111) surface. Reaction energetics were calculated in VASP using the VASPSol implicit solvation model. All reaction energetics are referenced to O-$NH_2$-DNT and the Au (111) surface in the solution phase at 0 V-RHE.

| Species | ΔG of reduction at 0 V-RHE (eV) |
|---|---|
| O-$NH_2$-DNT* (P-Ads) | 0.14 |
| P-NO-NAT* + OH* | 0.63 |
| P-NO-NAT* | -0.82 |
| P-NHO-NAT* | -1.31 |
| P-NHOH-NAT* | -1.77 |
| O-$NO_2$-DAT (aq) + OH* | -2.96 |
| O-$NO_2$-DAT (aq) | -4.41 |

**Figure S22:** Optimized geometries for reduced intermediates of P-$NH_2$-DNT to O-$NO_2$-DAT on the Au (111) surface. P-$NH_2$-DNT is adsorbed and reduced through the ortho group. Atom colors are presented as yellow: Au, grey: C, blue: N, red: O, and white: H.

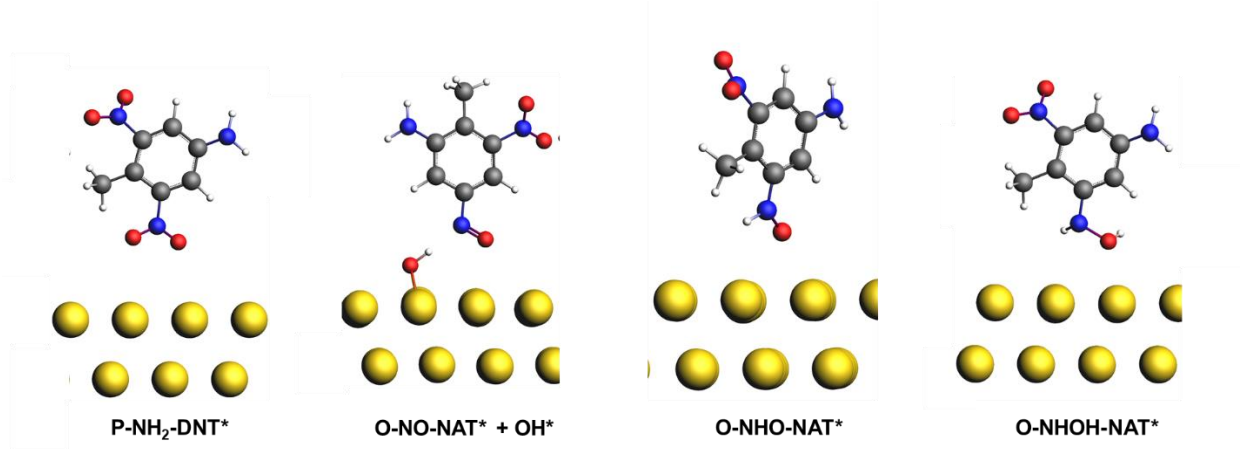


**Table S20:** Free energy change of reduction for the electrocatalytic reduction of P-$NH_2$-DNT to O-$NO_2$-DAT on the Au (111) surface. Reaction energetics were calculated in VASP using the VASPSol implicit solvation model. All reaction energetics are referenced to P-$NH_2$-DNT and the Au (111) surface in the solution phase at 0 V-RHE.

| Species | ΔG of reduction at 0 V-RHE (eV) |
|---|---|
| P-$NH_2$-DNT* (O ads) | 0.01 |
| P-NO-NAT* + OH* | 0.69 |
| P-NO-NAT* | -0.76 |
| P-NHO-NAT* | -1.38 |
| P-NHOH-NAT* | -1.86 |
| O-$NO_2$-DAT (aq) + OH* | -3.12 |
| O-$NO_2$-DAT (aq) | -4.57 |

**Figure S23:** Optimized geometries for reduced intermediates of P-$NO_2$-DAT to TAT on the Au (111) surface. P-$NO_2$-DAT is adsorbed and reduced through the para group. Atom colors are presented as yellow: Au, grey: C, blue: N, red: O, and white: H.

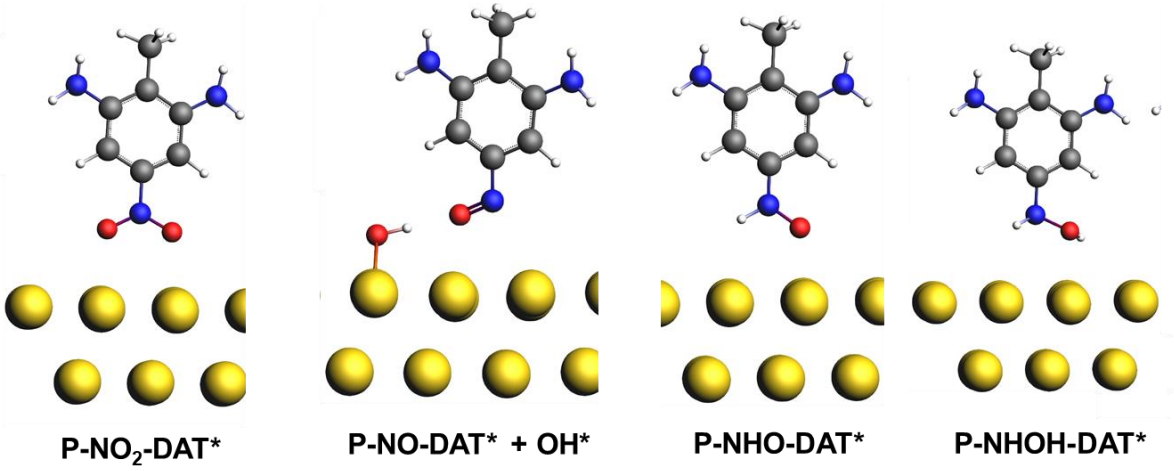


**Table S21:** Free energy change of reduction for the electrocatalytic reduction of P-$NO_2$-DAT to TAT on the Au (111) surface. Reaction energetics were calculated in VASP using the VASPSol implicit solvation model. All reaction energetics are referenced to P-$NO_2$-DAT and the Au (111) surface in the solution phase at 0 V-RHE.

| Species | ΔG of reduction at 0 V-RHE (eV) |
|---|---|
| P-$NO_2$-DAT* | 0.00 |
| P-NO-DAT +OH* | 0.52 |
| P-NO-DAT | -0.93 |
| P-NHO-DAT* | -1.11 |
| P-NHOH-DAT* | -1.55 |
| TAT (aq) + OH* | -2.54 |
| TAT (aq) | -3.99 |

**Figure S24:** Optimized geometries for reduced intermediates of O-$NO_2$-DAT to TAT on the Au (111) surface. O-$NO_2$-DAT is adsorbed and reduced through the ortho group. Atom colors are presented as yellow: Au, grey: C, blue: N, red: O, and white: H.

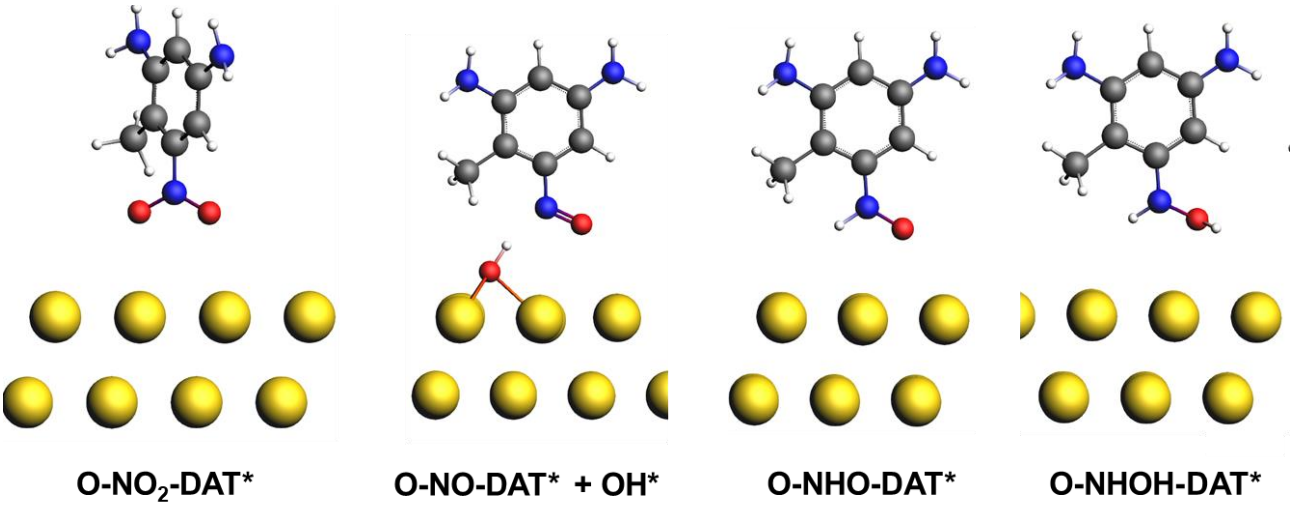


**Table S22:** Free energy change of reduction for the electrocatalytic reduction of O-$NO_2$-DAT to TAT on the Au (111) surface. Reaction energetics were calculated in VASP using the VASPSol implicit solvation model. All reaction energetics are referenced to O-$NO_2$-DAT and the Au (111) surface in the solution phase at 0 V-RHE.

| Species | ΔG of reduction at 0 V-RHE (eV) |
|---|---|
| O-$NO_2$-DAT* | 0.32 |
| O-NO-DAT +OH* | 0.82 |
| O-NO-DAT | -0.63 |
| O-NHO-DAT* | -1.03 |
| O-NHOH-DAT* | -1.63 |
| TAT (aq) + OH* | -2.41 |
| TAT (aq) | -3.85 |

**Figure S25:** Reaction energy diagram for electrocatalytic reduction of TNT to O-$NH_2$-DNT on the Au (111) surface at 0 V-RHE. Energies are relative to the bare solvated surface and TNT in the solution phase. TNT reduction is initiated through the flat adsorption configuration on the Au (111) surface. Water molecules formed during the reduction process are not listed on the diagram for clarity. Most stable configuration of each reduced intermediate are used to construct the reaction energy diagram. Water molecules formed during the reduction of TNT are not depicted for clarity. Black lines represent free energies of stable TNT intermediates. Atom colors are presented as yellow: Au grey: C, white: H, blue: N, and red: O.

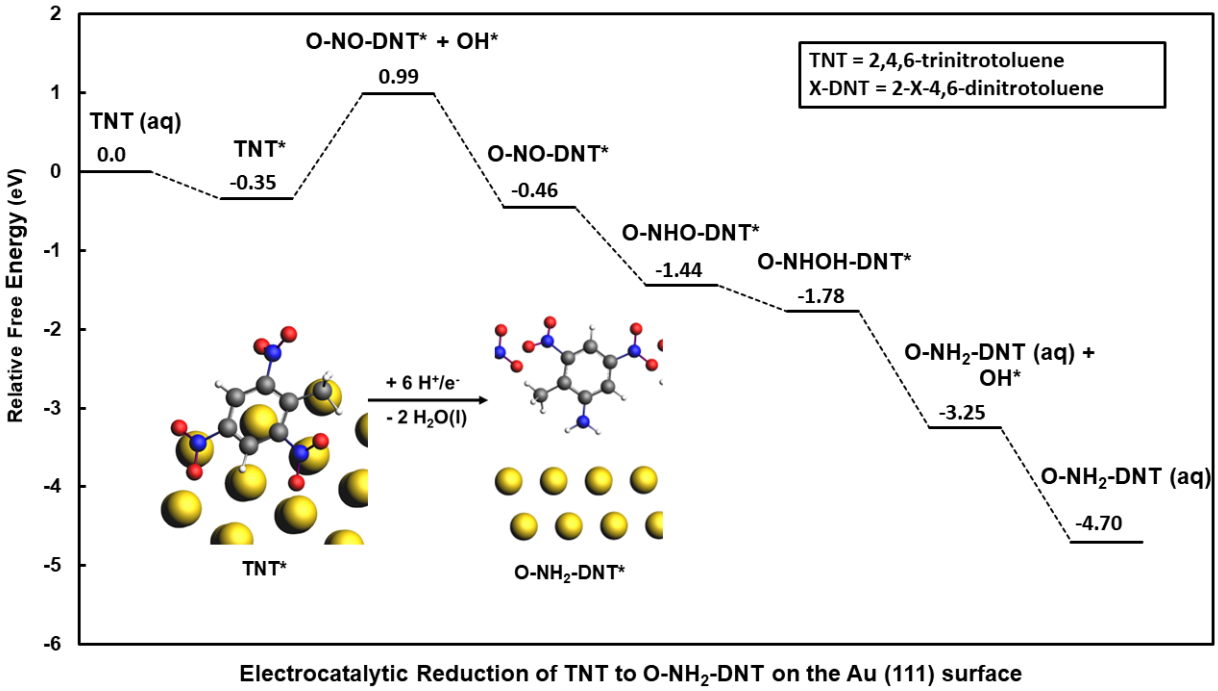


**Figure S26:** Optimized geometries for intermediates from TNT to O-$NH_2$-DNT reduction on the Au (111) surface. TNT is adsorbed in the flat configuration and reduced through the ortho group. Atom colors are presented as yellow: Au grey: C, white: H, blue: N, and red: O.

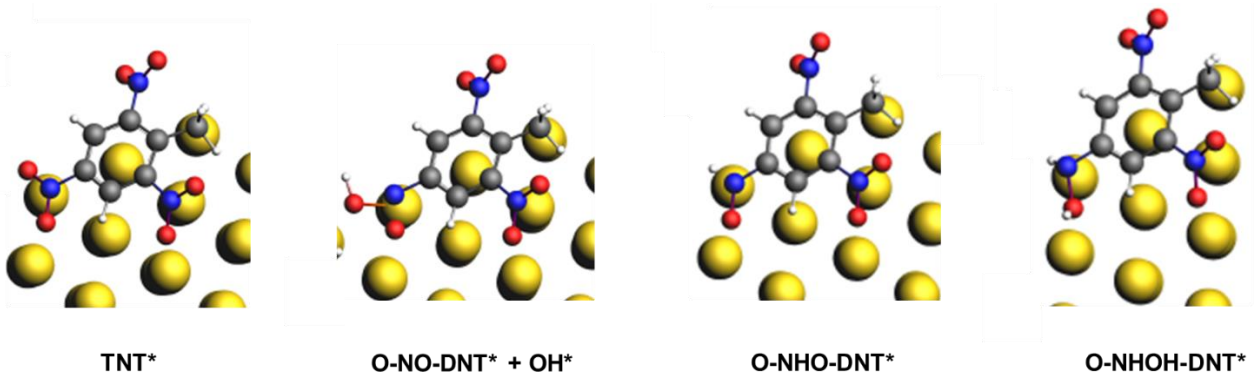

**Section S5: Potential dependent activation barriers for the initial reduction of TNT**

All activation barriers reported in this study are corrected to 0 V-RHE using a Butler-Volmer treatment. The equilibrium potential ($U_0$) for H* adsorption is calculated through the elementary reaction of adsorbing a bulk proton ($H^+(aq)$) on to the adsorption site on the metal surface ($*$) given in Eq. S1.

$$H^+(aq) + e^- + * \rightarrow H^* \quad (S1)$$

The free energy of the proton-electron pair can be approximated using the computational hydrogen electrode (CHE) approach, which equates the chemical potential of the proton-electron pair ($G_{H^+ + e^-}$) to the chemical potential of half of a hydrogen molecule ($G_{H_{2(aq)}}$) at 0 V-RHE and all pH values. This additionally accounts for the change in potential on a RHE scale by applying a linear shift of $|e^-|U_{RHE}$, where $e^-$is the charge of the electron and $U_{RHE}$ is the applied potential on an RHE scale. Therefore, the specific adsorption of H* can be written as the Gibbs free energy of adsorption as a function of $U_{RHE}$

$$\Delta G_{ads}(U_{abs}) = G_{H*} - G_* - \frac{1}{2}G_{H_{2(aq)}} + |e^-|U_{RHE} \quad (S2)$$

where $G_{H*}$, $G_*$, and $G_{H_{2(aq)}}$ are respectively the free energy of the surface adsorbed proton, available adsorption site, and the hydrogen atom in the solution phase. The equilibrium potential on an RHE scale, $U^0_{RHE}$, can be determined at equilibrium ($\Delta G_{ads}(U^0_{RHE}) = 0$) in Eq. S3.

$$U^0_{RHE} = \frac{-G_{H*} + G_* + \frac{1}{2}G_{H_{2(aq)}}}{|e^-|} \quad (S3)$$

DFT reported equilibrium adsorption potentials of H* and potential dependent activation barriers are reported in **Table S23.**

**Table S23:** Equilibrium adsorption potentials of H* and activation barriers of TNT* to NO-DNT* + OH* on Fe (110), Cu (111), Pt (111), and Au (111) surfaces. $U_0$ of H* adsorption are reported on a RHE scale. Activation barriers are corrected to 0 V-RHE.

| **Metal Surface** | **H* adsorption equilibrium potential (V-RHE)** | **Activation barrier of $NO_2$-DNT* to NO-DNT* + OH* (eV)** |
|---|---|---|
| Fe (110) | 0.66 | -0.32 |
| Au (111) | 0.12 | 1.13 |
| Pt (111) | 0.38 | 0.53 |
| Cu (111) | -0.25 | 0.58 |

Due to the linear extrapolation of the Butler-Volmer approach, the activation barrier on the Fe (110) surface is negative at 0 V-RHE. This indicates that the activation barrier is approximately zero (barrierless) at potentials slightly higher than 0 V-RHE.

**Section S6: TNT reduction intermediates across M late transition metal surfaces**

The binding energy of O*, free energy change of initial R-$NO_2$ and OH* reduction, and DFT predicted limiting potentials across monometallics and bimetallics are reported in Table S24.

**Table S24:** O* binding energies and free energy changes of initial R-$NO_2$ reduction and OH* reduction across monometallic, bimetallic, and partially reduce $Fe_2O_3$ (0001) surfaces. Reaction energetics are relative to solution phase species and the solvated bare metal surface.

| Metal Surface | Binding energy of O* | ΔG of TNT* → NO-DNT* + OH* (eV) | ΔG of OH* → $H_2O$ (l) (eV) | Limiting Potential (V-RHE) |
|---|---|---|---|---|
| Au (111) | -2.10 | -1.45 | 0.63 | -0.63 |
| Ag (111) | -2.52 | -1.01 | -0.29 | 0.29 |
| Pt (111) | -3.31 | -0.96 | -0.48 | 0.48 |
| Pd (111) | -3.54 | -0.53 | -0.56 | 0.53 |
| Cu (111) | -3.60 | -0.54 | -0.57 | 0.54 |
| Ir (111) | -3.73 | -0.63 | -0.58 | 0.58 |
| Rh (111) | -4.21 | -0.37 | -1.29 | 0.37 |
| Ni (111) | -4.47 | -0.27 | -1.39 | 0.27 |
| Ru (0001) | -4.76 | -0.01 | -1.49 | 0.01 |
| Co (0001) | -5.30 | 0.09 | -2.00 | -0.09 |
| Fe (110) | -5.53 | 0.75 | -2.45 | -0.75 |
| Ni/Cu (111) | -3.65 | -0.61 | -1.50 | 0.61 |
| Pd/Cu (111) | -3.17 | -0.55 | -0.15 | 0.15 |
| Pt/Cu (111) | -3.54 | -0.32 | -0.25 | 0.40 |
| Ir/Cu (111) | -3.43 | -0.49 | -0.65 | 0.32 |
| Rh/Cu (111) | -3.89 | -0.40 | -1.74 | 0.49 |
| $Fe_2O_3$ (0001) | -5.15 | 1.54 | -0.88 | -1.54 |
| Ni/$Fe_2O_3$ (0001) | -4.94 | -1.06 | 1.23 | -1.23 |

**Figure S27:** Optimized geometries of TNT* and O-NO-DNT* + OH* across monometallic surfaces. Adsorbate atom colors are as follows: grey = C, blue = N, red = O, and white = H.

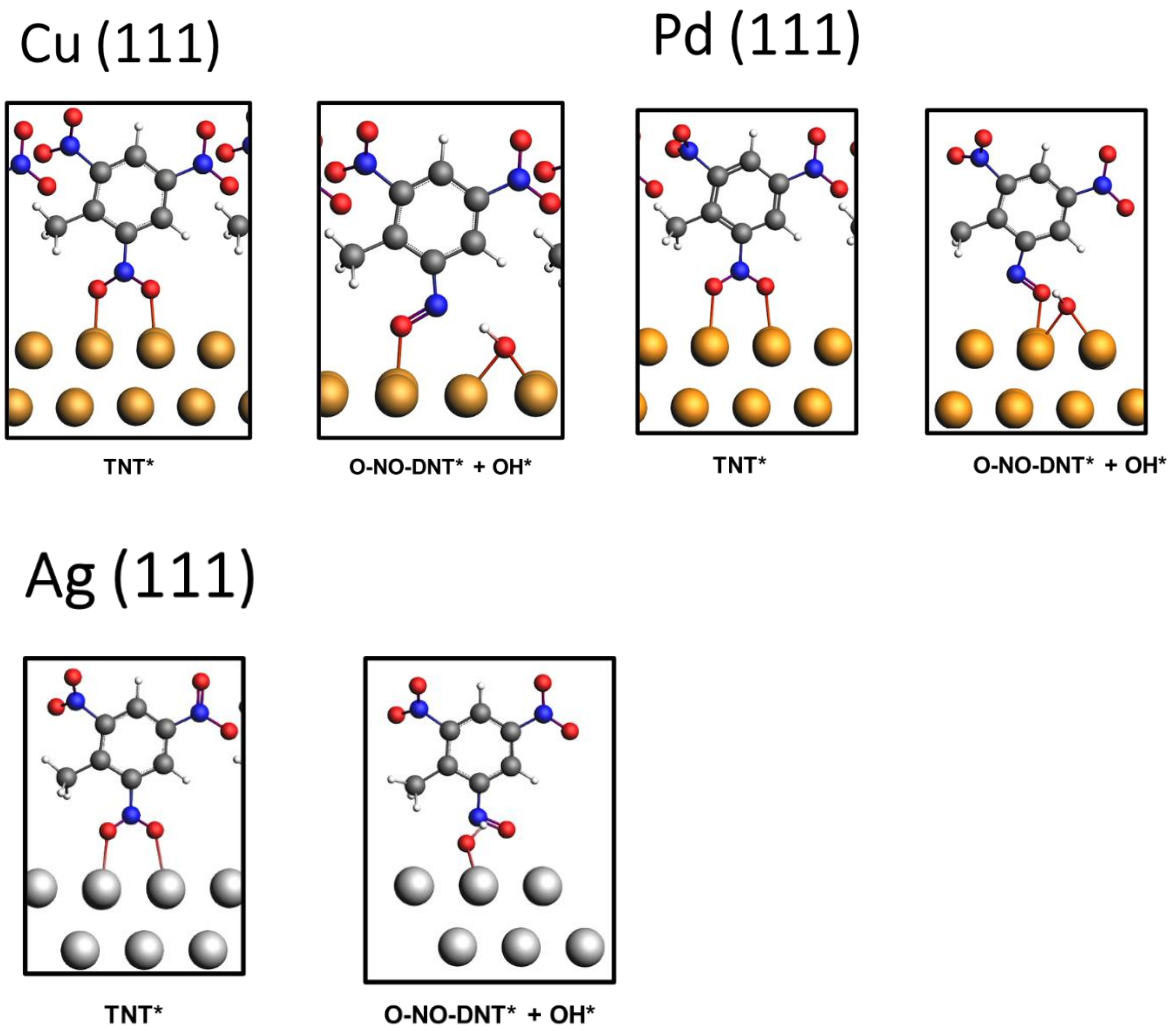

## Ni (111)

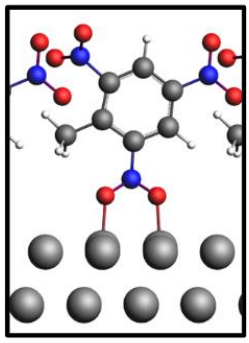

TNT*

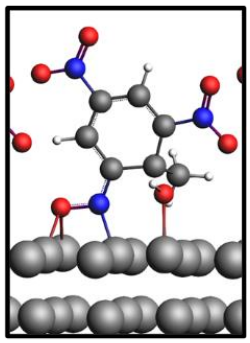

O-NO-DNT* + OH*

## Rh (111)

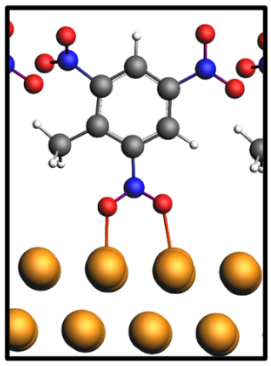

TNT*

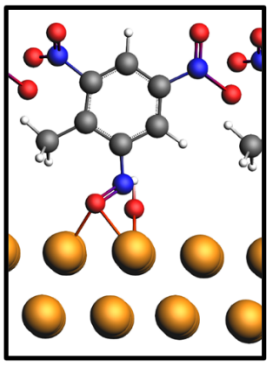

O-NO-DNT* + OH*

## Ir (111)

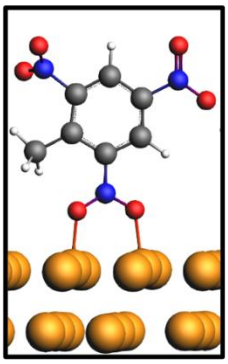

TNT*

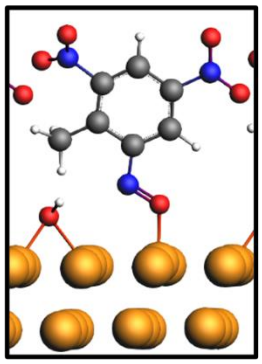

O-NO-DNT* + OH*

## Co (0001)

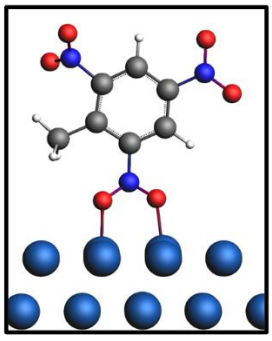

TNT*

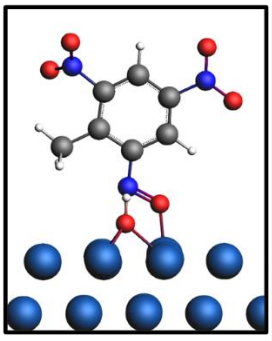

O-NO-DNT* + OH*

## Ru (0001)

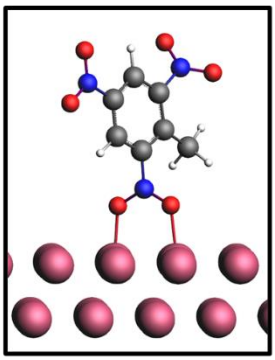

TNT*

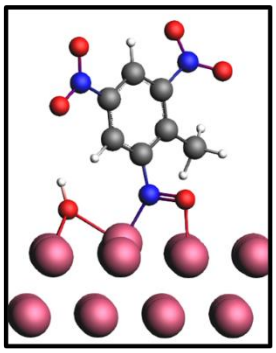

O-NO-DNT* + OH*

**Section 7: TNT reduction on Bimetallic X/Cu (111) late transition metal surfaces**

**Figure S28:** Optimized geometries of TNT* and O-NO-DNT* + OH* on X/Cu (111) surfaces. Atom colors of the adsorbates are as follows: grey = C, blue = N, red = O, and white = H.

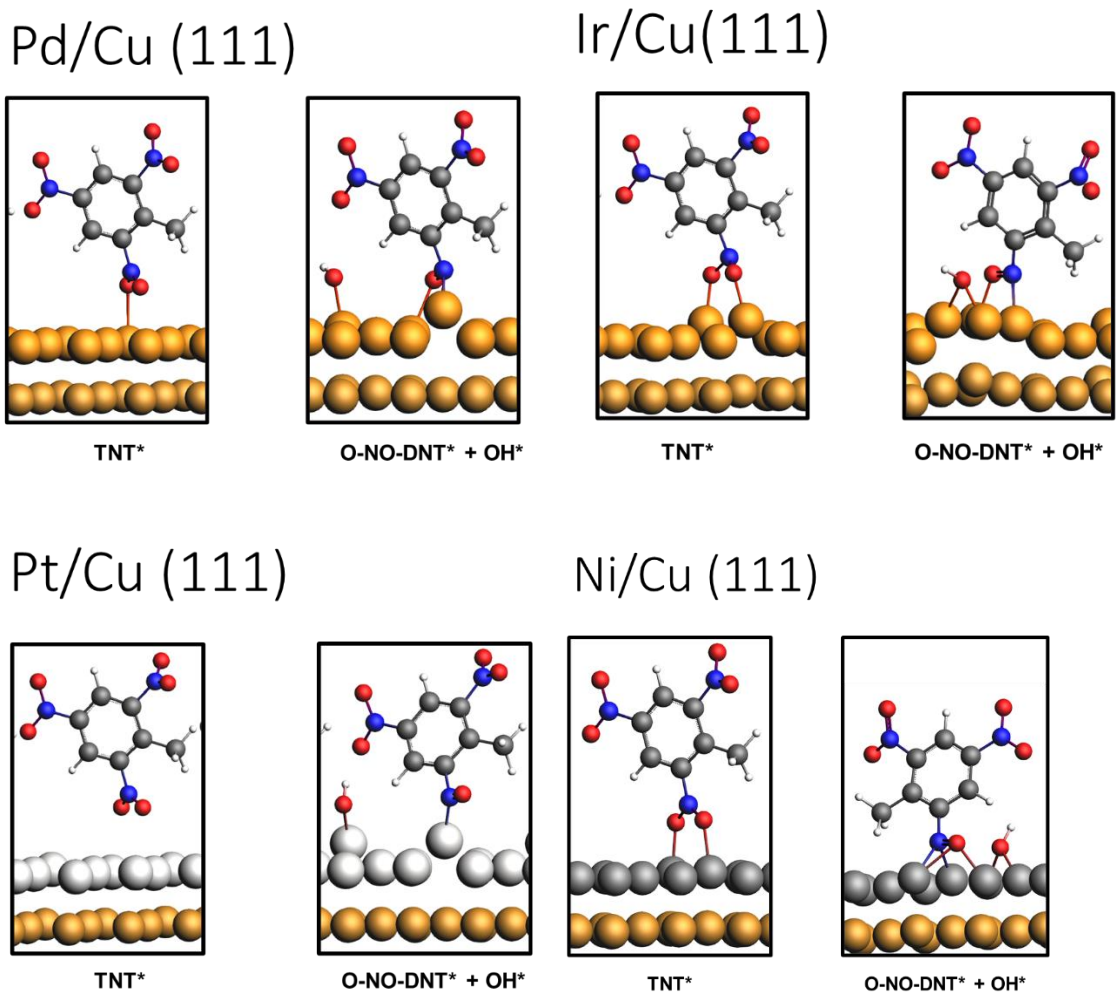

# Rh/Cu (111)

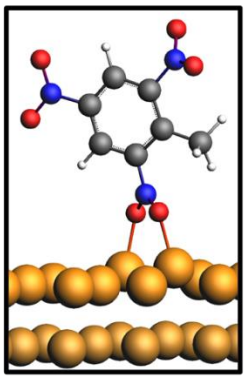

TNT*

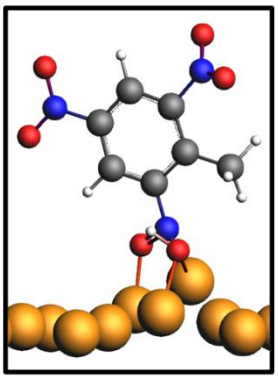

O-NO-DNT* + OH*

**Table S25:** Binding energies of O* on bimetallic surfaces relative to that on the Pt (111) surface. O* binding energies are reported from Greeley et al.[1] First three columns indicate the surface atom type. The last column is the atom type of the two substrate layers in the three-layer slabs. All surface models are closed-packed where the lattice constant is dictated by the substrate atoms.

| Surf 1 | Surf 2 | Surf 3 | Substrate atoms | $\Delta(BE_O\text{-}BE_{\text{-}O}\text{-Pt (111)})$ |
|---|---|---|---|---|
| Cu | Cu | Bi | Cu | 0 |
| Ag | Ag | Ag | Re | -0.01 |
| Au | Cd | Cd | Au | -0.01 |
| Ir | Sb | Sb | Ir | -0.02 |
| Au | Au | Co | Co | -0.02 |
| As | As | Fe | Fe | -0.03 |
| Bi | Bi | Bi | Ag | -0.03 |
| Pd | Cd | Cd | Pd | -0.03 |
| Ru | Sb | Sb | Ru | -0.03 |
| Pd | Pd | Sb | Pd | -0.04 |
| Pt | Pt | Au | Pt | -0.04 |
| Pd | As | As | Pd | -0.04 |
| Pt | As | As | Pt | -0.05 |
| Pt | Pt | Au | Au | -0.05 |
| Pt | Ag | Ag | Ag | -0.06 |
| Pd | Pd | Pd | Rh | -0.06 |
| Ni | Sb | Sb | Ni | -0.07 |
| Pd | Pd | Ag | Ag | -0.07 |
| Ag | Ag | Cd | Ag | -0.08 |
| Au | Au | Au | Bi | -0.09 |
| Cu | Bi | Bi | Cu | -0.11 |
| Ag | Ag | Ag | Cd | -0.11 |
| Cd | Cd | Cd | Rh | -0.11 |
| As | As | As | Pd | -0.11 |
| Pd | Pd | Cd | Pd | -0.11 |
| Pd | Pd | Pd | Ru | -0.11 |
| Pt | Cu | Cu | Cu | -0.12 |
| Ag | Bi | Bi | Ag | -0.12 |
| Pt | Ag | Ag | Pt | -0.12 |
| Cu | As | As | Cu | -0.12 |
| Ru | As | As | Ru | -0.13 |
| Cd | Cd | Cd | Ir | -0.13 |
| Pd | Pd | Pd | Ir | -0.14 |

| | | | | |
|---|---|---|---|---|
| Ni | Ni | Bi | Ni | -0.15 |
| Cu | Cd | Cd | Cu | -0.16 |
| Pd | Pd | Ag | Pd | -0.16 |
| Pt | Cd | Cd | Pt | -0.17 |
| Pt | Pt | As | Pt | -0.17 |
| Cd | Cd | Cd | Re | -0.17 |
| Pt | Pt | Ag | Ag | -0.18 |
| Co | Sb | Sb | Co | -0.18 |
| As | As | As | Pt | -0.2 |
| Ag | Ag | Sb | Ag | -0.21 |
| Cu | Cu | Sb | Cu | -0.23 |
| Cd | Cd | Cd | Ru | -0.23 |
| Pd | Pd | Ni | Ni | -0.25 |
| Rh | Au | Au | Rh | -0.25 |
| Pt | Pt | Fe | Fe | -0.26 |
| Ru | Bi | Bi | Ru | -0.26 |
| Bi | Bi | Bi | Au | -0.27 |
| Ag | Cd | Cd | Ag | -0.27 |
| Pt | Pt | Cd | Pt | -0.28 |
| Pt | Pt | Pt | Ag | -0.29 |
| Ag | Ag | Ag | Sb | -0.29 |
| Au | Au | As | Au | -0.29 |
| Sb | Sb | Sb | Ag | -0.3 |
| Fe | Sb | Sb | Fe | -0.3 |
| Cu | Cu | As | Cu | -0.31 |
| Au | Au | Bi | Bi | -0.31 |
| Rh | Rh | Bi | Rh | -0.32 |
| Au | Sb | Sb | Au | -0.32 |
| Pd | Cu | Cu | Cu | -0.33 |
| Au | Au | Fe | Fe | -0.33 |
| Cd | Cd | Cd | Pt | -0.33 |
| Pd | Pd | Pd | Ag | -0.34 |
| Pt | Pt | Pt | As | -0.34 |
| Ir | Bi | Bi | Ir | -0.34 |
| Pt | Pt | Ag | Pt | -0.35 |
| Pd | Pd | As | Pd | -0.35 |
| Ag | Ag | Ni | Ni | -0.36 |
| Ni | Ni | Sb | Ni | -0.36 |

| | | | | |
|---|---|---|---|---|
| Pt | Pt | Pt | Pd | -0.37 |
| Ag | Ag | Cd | Cd | -0.37 |
| Cd | Cd | Cd | Pd | -0.37 |
| Pt | Pt | Rh | Rh | -0.38 |
| Pd | Pd | Pd | As | -0.38 |
| Cu | Sb | Sb | Cu | -0.38 |
| Cu | Cu | Ag | Cu | -0.4 |
| Au | Cd | Cd | Cd | -0.4 |
| Rh | Au | Au | Au | -0.42 |
| Ir | As | As | Ir | -0.42 |
| Pt | Pt | As | As | -0.42 |
| Pt | Pt | Pt | Pt | -0.42 |
| Ag | Ag | As | Ag | -0.43 |
| Cu | Ag | Ag | Ag | -0.43 |
| Fe | Bi | Bi | Fe | -0.45 |
| Au | Au | Ni | Au | -0.45 |
| Rh | Cd | Cd | Rh | -0.45 |
| Pt | Pt | Ru | Ru | -0.45 |
| Sb | Sb | Sb | Au | -0.46 |
| Pd | Pd | Pd | Au | -0.46 |
| Pt | Pt | Pt | Au | -0.47 |
| Cd | Cd | Ni | Ni | -0.47 |
| Rh | Rh | Sb | Rh | -0.47 |
| Pt | Pt | Pd | Pd | -0.47 |
| Bi | Bi | Bi | Cd | -0.47 |
| Ag | Sb | Sb | Ag | -0.47 |
| Pd | Pd | Pd | Pd | -0.48 |
| Co | Co | Bi | Co | -0.5 |
| Pd | Pd | Co | Co | -0.51 |
| As | Ni | Ni | Ni | -0.51 |
| Pt | Pt | Pd | Pt | -0.51 |
| Au | Au | Sb | Sb | -0.52 |
| Au | Au | As | As | -0.52 |
| Au | Ni | Ni | Ni | -0.52 |
| Pd | Pd | Cd | Cd | -0.53 |
| Pt | Pd | Pd | Pd | -0.53 |
| Pd | Pd | Pd | Pt | -0.53 |
| Ru | Ru | Bi | Ru | -0.54 |

| | | | | |
|---|---|---|---|---|
| Pd | Cd | Cd | Cd | -0.54 |
| Cu | Cu | Cd | Cu | -0.55 |
| Rh | Rh | As | Rh | -0.56 |
| Ag | Ag | As | As | -0.56 |
| Ru | Au | Au | Ru | -0.57 |
| Pt | Pd | Pd | Pt | -0.58 |
| Au | As | As | Au | -0.58 |
| Pt | Cd | Cd | Cd | -0.58 |
| Ag | Ag | Ag | Bi | -0.59 |
| Cd | Cd | Cd | As | -0.6 |
| Ir | Ir | Sb | Ir | -0.6 |
| Ir | Ir | Ir | Co | -0.6 |
| Cd | Cd | Cd | Ag | -0.61 |
| Co | Co | Sb | Co | -0.61 |
| Bi | Bi | Bi | As | -0.62 |
| Rh | Rh | Au | Rh | -0.62 |
| Cd | Cd | Cd | Au | -0.63 |
| As | Co | Co | Co | -0.63 |
| Cd | Bi | Bi | Cd | -0.63 |
| Pt | Pt | Ir | Ir | -0.63 |
| Ru | Ru | Sb | Ru | -0.64 |
| Pt | Ni | Ni | Ni | -0.64 |
| Pd | Pd | Cu | Pd | -0.66 |
| Ag | As | As | Ag | -0.66 |
| Pd | Pd | As | As | -0.67 |
| Ru | Ru | As | Ru | -0.67 |
| Cu | Cu | Au | Au | -0.68 |
| Pt | Pt | Cu | Pt | -0.69 |
| Ag | Cd | Cd | Cd | -0.7 |
| Cu | Cu | Cu | Ni | -0.7 |
| Rh | Pd | Pd | Rh | -0.7 |
| Ir | Ir | Ir | Ni | -0.71 |
| As | As | As | Ag | -0.72 |
| Ir | Ir | Au | Ir | -0.74 |
| Cu | Cu | Cu | Co | -0.75 |
| Pt | Pt | Cd | Cd | -0.75 |
| Rh | Cu | Cu | Cu | -0.75 |
| Pt | As | As | As | -0.76 |

| | | | | |
|---|---|---|---|---|
| Ru | Au | Au | Au | -0.76 |
| Au | As | As | As | -0.78 |
| Ag | Ag | Bi | Bi | -0.78 |
| As | Sb | Sb | As | -0.78 |
| Ag | Ag | Co | Co | -0.78 |
| Pd | Pd | Fe | Fe | -0.79 |
| Au | Au | Co | Au | -0.79 |
| Ir | Ir | Ir | Fe | -0.79 |
| Cd | Cd | Bi | Cd | -0.81 |
| Ir | Ir | Bi | Ir | -0.81 |
| Cu | Cu | Cu | Cu | -0.81 |
| Sb | Sb | Sb | As | -0.82 |
| Sb | Sb | Sb | Cd | -0.83 |
| Rh | Ag | Ag | Ag | -0.83 |
| Au | Au | Fe | Au | -0.83 |
| Au | Bi | Bi | Bi | -0.83 |
| Ru | Ru | Au | Ru | -0.84 |
| Ir | Ir | Cu | Cu | -0.84 |
| Ru | As | As | As | -0.84 |
| Rh | Ag | Ag | Rh | -0.86 |
| Pd | Pd | Pd | Cd | -0.86 |
| Ir | Ir | Ni | Ni | -0.87 |
| Ru | Pd | Pd | Ru | -0.87 |
| Pt | Ir | Ir | Ir | -0.88 |
| As | As | Bi | As | -0.88 |
| Pd | Cu | Cu | Pd | -0.89 |
| As | Bi | Bi | As | -0.89 |
| Rh | As | As | As | -0.89 |
| As | As | As | Au | -0.9 |
| Pd | Pd | Pd | Sb | -0.9 |
| Pt | Co | Co | Co | -0.91 |
| As | As | Sb | As | -0.91 |
| Ru | Cu | Cu | Cu | -0.91 |
| Ir | Cu | Cu | Cu | -0.92 |
| Fe | Fe | Sb | Fe | -0.92 |
| Pt | Rh | Rh | Rh | -0.92 |
| Ir | As | As | As | -0.92 |
| Cd | Cd | Co | Co | -0.93 |

| | | | | |
|---|---|---|---|---|
| Ag | Ag | Sb | Sb | -0.93 |
| Cd | Cd | Cd | Cd | -0.93 |
| Pd | As | As | As | -0.93 |
| Pd | Pd | Bi | Bi | -0.93 |
| Au | Co | Co | Co | -0.93 |
| Cu | Cu | Cu | Fe | -0.94 |
| Pt | Cu | Cu | Pt | -0.94 |
| Rh | Rh | Cd | Rh | -0.94 |
| Rh | Rh | Cu | Cu | -0.94 |
| Rh | Rh | Rh | Co | -0.95 |
| As | Fe | Fe | Fe | -0.96 |
| Pd | Ni | Ni | Ni | -0.96 |
| Pt | Pt | Sb | Sb | -0.96 |
| Pt | Pt | Rh | Pt | -0.97 |
| Ir | Ir | Ir | Re | -0.97 |
| Pd | Pd | Pd | Bi | -0.97 |
| Ir | Ir | As | Ir | -0.97 |
| Cu | Cu | Ag | Ag | -0.98 |
| Ir | Ir | Co | Co | -0.98 |
| Ag | As | As | As | -0.98 |
| Pd | Pd | Sb | Sb | -0.98 |
| Ru | Cd | Cd | Ru | -0.99 |
| Pt | Pt | Ru | Pt | -0.99 |
| Ir | Au | Au | Ir | -1 |
| Ir | Ir | Cd | Ir | -1 |

**Section S8: TNT reduction intermediates on partially reduced $Fe_2O_3$ (00001) metal surfaces**

**Figure S29:** Optimized geometries of bare partially reduced $Fe_2O_3$ (0001) surface (with Ni doping). Atom colors are as follows: brown = Fe, red = O, white = H, grey = Ni.

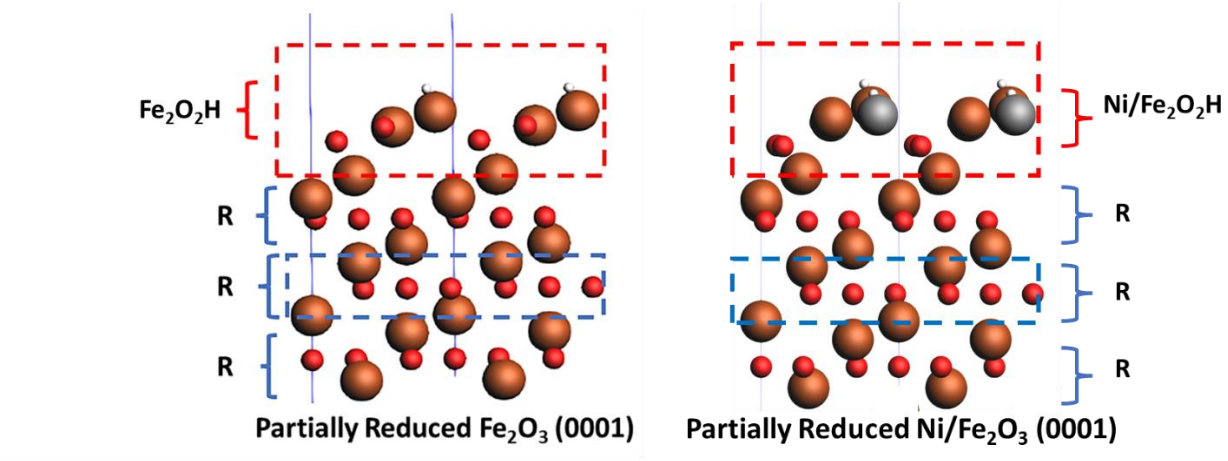


**Figure S30:** Optimized geometries of bare partially reduced $Fe_2O_3$ (0001) surface (with Ni doping). Atom colors are as follows: brown = Fe, red = O, white = H, grey = Ni.

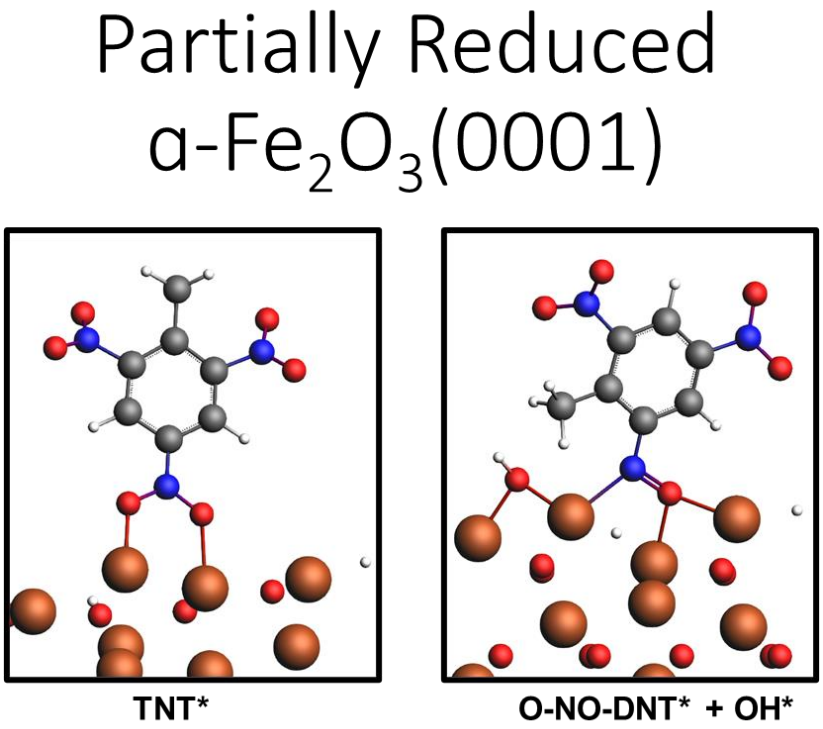

# Partially Reduced α-Ni/$Fe_2O_3$(0001)

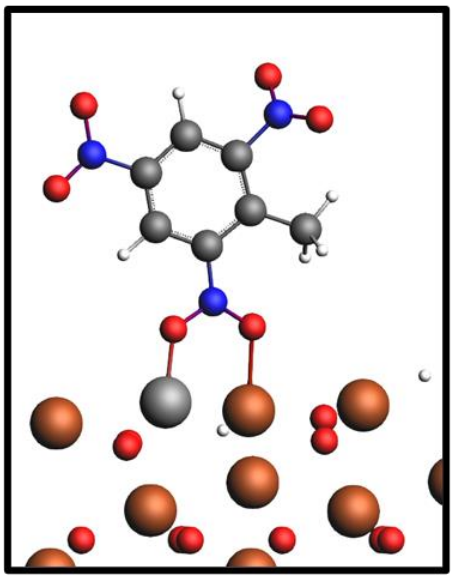

TNT*

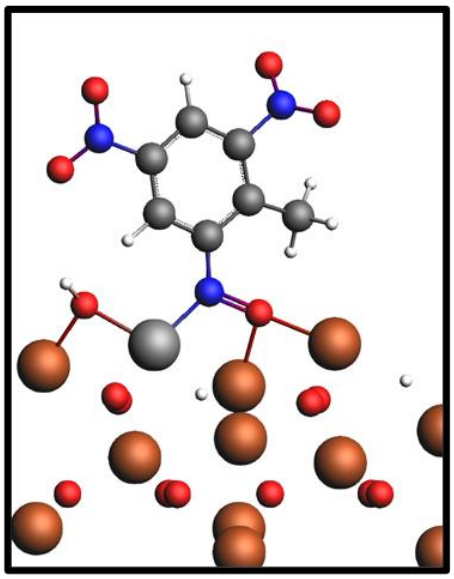

O-NO-DNT* + OH*

**References:**

[1] J. Greeley, J.K. Nørskov, Combinatorial Density Functional Theory-Based Screening of Surface Alloys for the Oxygen Reduction Reaction, J. Phys. Chem. C. 113 (2009) 4932–4939. https://doi.org/10.1021/jp808945y.